

Influence of atmospheric deposition on biogeochemical cycles in an oligotrophic ocean system

France Van Wambeke¹, Vincent Taillandier², Karine Desboeufs³, Elvira Pulido-Villena¹, Julie Dinasquet^{4,5}, Anja Engel⁶, Emilio Marañón⁷, Céline Ridame⁸, Cécile Guieu²

5

¹ Aix-Marseille Université, CNRS/INSU, Université de Toulon, IRD, Mediterranean Institute of Oceanography (MIO) UM 110, 13288, Marseille, France

² CNRS, Sorbonne Université, Laboratoire d'Océanographie de Villefranche (LOV), UMR7093, 06230 Villefranche-sur-Mer, France

10 ³ LISA, UMR CNRS 7583, Université Paris-Est-Créteil, Université de Paris, Institut Pierre Simon Laplace (IPSL), Créteil, France

⁴ Sorbonne Universités, Laboratoire d'Océanographie Microbienne (LOMIC), Observatoire Océanologique, 66650, Banyuls/mer, France

⁵ Marine Biology Research Division, Scripps Institution of Oceanography, UCSD, La Jolla, USA

15 ⁶ GEOMAR – Helmholtz-Centre for Ocean Research, Kiel, Germany

⁷ Department of Ecology and Animal Biology, Universidade de Vigo, 36310 Vigo, Spain

⁸ Sorbonne University/CNRS/IRD/MNHN, LOCEAN: Laboratoire d'Océanographie et du Climat: Expérimentation et Approches Numériques, UMR 7159, 4 Place Jussieu – 75252 Paris Cedex 05, France

Correspondence to: France Van Wambeke (france.van-wambeke@mio.osupytheas.fr) and
20 Cécile Guieu (guieu@imev-mer.fr)

Abstract.

The surface mixed layer (ML) in the Mediterranean Sea is a well stratified domain characterized by low macro-nutrients and low chlorophyll content, for almost 6 months of the year. In this study we characterize the biogeochemical cycling of N in the ML by analysing

25 simultaneous *in situ* measurements of atmospheric deposition, nutrients, hydrological conditions, primary production, heterotrophic prokaryotic production, N_2 fixation and leucine aminopeptidase activity. Dry deposition was continuously measured across the central and western open Mediterranean Sea and two wet deposition events were sampled, one in the Ionian Sea and one in the Algerian basin. Along the transect, N budgets were computed to
30 compare the sources and sinks of N in the mixed layer. *In situ* leucine aminopeptidase activity made up 14 to 66 % of the heterotrophic prokaryotic N demand, and the N_2 fixation rate represented 1 to 4.5 % of the phytoplankton N demand. Dry atmospheric deposition of

inorganic nitrogen, estimated from dry deposition of (nitrate+ammonium) in aerosols, was higher than the N₂ fixation rates in the ML (on average 4.8-fold). The dry atmospheric input of inorganic N represented a highly variable proportion of biological N demand in the ML among the stations, 10 - 82% for heterotrophic prokaryotes and 1-30% for phytoplankton. As some sites were visited for several days the evolution of biogeochemical properties in the ML and within the nutrient-depleted layers could be followed. At the Algerian Basin site, the biogeochemical consequences of a wet dust deposition event was followed with a high frequency sampling of CTD casts. Notably just after the rain, nitrate was higher in the ML than in the nutrient depleted layer below. Estimates of nutrient transfer from the ML to the nutrient depleted layer could explain up to a 1/3 of the nitrate loss from the ML. Phytoplankton did not benefit directly from the atmospheric inputs into the ML, probably due to high competition with heterotrophic prokaryotes, also limited by N and P availability at the time of this study. Primary producers decreased their production after the rain, recovering to their initial state of activity after a 2 day lag in the vicinity of the deep chlorophyll maximum layer.

1. Introduction

The Mediterranean Sea (MS) is a semi-enclosed basin characterized by very short ventilation and residence times due to its own thermohaline circulation (Mermex Group, 2011). ~~In terms of biogeochemistry, the MS is characterized by a long summer stratification period.~~ It is a low nutrient, low chlorophyll (LNLC) system with ~~where there is generally an increasing~~ oligotrophic gradient from west to east and ~~an overall~~ deficit in phosphorus (P) compared to nitrogen (N) (Mermex Group, 2011). This is confirmed by ~~an~~ N/P ratio for inorganic nutrients ~~that is higher than the Redfield ratio in deep layers, which~~ increases toward the east (Krom et al., 2004).

The relationship between photoautotrophic unicellular organisms and heterotrophic prokaryotes (competition or commensalism) is affected by the balance of light and nutrients as well as possible inputs of organic matter from river runoff or atmospheric deposition. Phytoplankton generally experience P, N, or NP limitation (Thingstad et al., 2005 ; Tanaka et al., 2011, Richon et al., 2018), whereas heterotrophic prokaryotes are usually P limited, or P and labile carbon co-limited (Sala et al., 2002, Van Wambeke et al., 2002, Céa et al., 2014). The MS receives anthropogenic aerosols ~~continuously~~, originating from industrial and domestic activities from around the basin and from other parts of Europe along with pulsed natural inputs from the Sahara. It is thus a natural LNLC study area, well adapted to

investigate the role of ocean–atmosphere exchanges of particles and gases on marine biogeochemical cycles. ~~Parameterization and representation of the key processes brought into play by atmospheric deposition in the MS must take into account the role of pulsed atmospheric inputs (Guieu et al., 2014a)~~. Recent studies describe annual records of atmospheric deposition of trace metals and inorganic macronutrients (N, P) obtained at several locations around the MS (Markaki et al., 2010; Guieu and Ridame, in press; Desboeufs, in press). All records ~~denote the~~ pulsed and highly variable inputs. Recent models and observations show that atmospheric deposition of organic matter (OM) is also highly variable and that their annual inputs are of the same order of magnitude as river inputs (Djaoudi et al., 2017, Kanakidou et al., 2018; Kanakidou et al., 2020; Galetti et al., 2020). Moreover, the sum of atmospheric inputs of nitrate, ammonium and soluble organic nitrogen has been shown to be equivalent or higher than those of N₂ fixation rates (Sandroni et al., 2007), although inorganic atmospheric N inputs alone may also be higher than N₂ fixation rates (Bonnet et al., 2011).

Aerosol amendments in bottles, minicosms or mesocosms have been widely used to study trophic transfer and potential export, as they ~~represent to some extent a ‘simplified’ plankton trophic web that can be studied along a vertical dimension~~ (i.e. Guieu et al., 2010; Herut et al., 2016; Mescioglu et al., 2019). ~~It has been shown that~~ both diversity and functioning of various biological compartments are impacted by aerosol additions in different waters tested in the MS (Guieu and Ridame, in press, and synthesis Figure 3 therein). Differences in the biological responses have been observed, depending on the mode of deposition simulated (wet or dry), the type of aerosols used (natural or anthropogenic) and the *in situ* biogeochemical conditions at the time of the experiment (Guieu and Ridame, in press). Organic carbon from aerosols is partly soluble, and this soluble fraction is partly available to marine heterotrophic prokaryotes (Djaoudi et al., 2020). Heterotrophic prokaryotes have the metabolic capacity to respond quickly to aerosol deposition through growth and changes in community composition (Rahav et al., 2016; Pulido-Villena et al., 2008; 2014), while the phytoplankton community responds more slowly or not at all (Guieu and Ridame, in press, and reference therein).

Owing to the intrinsic experimental limitations, which vary depending on the size and design of enclosures (i.e. the omission of higher trophic levels, absence of turbulent mixing so limiting exchanges by diffusion, and wall effects) such experiments cannot fully simulate *in situ* conditions (Guieu and Ridame, in press). Thus, ~~it is still necessary to acquire~~ *in situ*

observations to understand the consequences of aerosol deposition on biogeochemical cycles.

100 Such *in situ* studies are scarce and require dedicated high frequency sampling to follow the effects of deposition on the biogeochemical processes while taking into account the water column dynamics. To demonstrate this point, the biological response to a Saharan dust event (dust flux = 2.6 g m^{-2} recorded at a coastal station in Cap Ferrat) was detected 4 days after the event by only one offshore water column sampling (at the DYFAMED site). An increase in 105 heterotrophic prokaryotic respiration and abundance was observed when compared to a sampling that was carried out 16 days before this dust event (Pulido-Villena et al., 2008). Off the Israeli coast a moderate natural dust storm (1.05 mg L^{-1} over 5 m depth) was followed every 12 hours over 5 days (Rahav et al., 2016). Rapid changes were observed, which could have been missed without high frequency sampling. A decrease in picophytoplankton 110 abundance, an increase in heterotrophic prokaryote abundance, as well as a slight increase in primary production (25%) and heterotrophic prokaryotic production (15%) was observed. Hence, it is necessary to organize sampling surveys with adaptive strategies to follow aerosol deposition events *in situ* and their impacts on biogeochemical processes, especially in the open waters of the stratified and nutrient limited MS. The objectives of the PEACTIME 115 project were to study fundamental processes and their interactions at the ocean–atmosphere interface following atmospheric deposition (especially of Saharan dust) in the Mediterranean Sea, and how these processes impact the functioning of the pelagic ecosystem (Guieu et al., 2020).

120 As atmospheric deposition affects primarily the surface mixed layer (ML), the present study focuses on the upper part of the nutrient depleted layer that extends down to the nutriclines (as defined by Du et al., 2017). During the stratification period, concentrations of nitrate and phosphate inside the ML are often below the quantification limits of standard methods. However, nanomolar concentrations of nitrate (and phosphate) can now be assessed 125 accurately through the Long Waveguide Capillary Cell (LWCC) technique (Zhang and Chi, 2002), which permits the measurement of fine gradients inside nutrient depleted layers of the MS (Djaoudi et al., 2018).

130 The aims of the present study were to assess the impact of atmospheric nutrient deposition on biogeochemical processes and fluxes in the open sea during the PEACTIME cruise in the MS. For this we i) estimated nanomolar variations of nitrate concentrations in the surface mixed layer (ML) facing variable inputs of dry and wet aerosol deposition and ii) we compared the aerosol-derived N inputs to the ML with biological activities: primary production,

heterotrophic prokaryotic production, N₂ fixation and ectoenzymatic activity (leucine aminopeptidase). We studied the N budgets along a transect, to include 13 stations crossing the Algerian Basin, Tyrrhenian Sea and the Ionian Sea where dry atmospheric deposition was 135 continuously measured on board together with seawater biogeochemical, biological and physical characteristics. We finally focused on a high frequency sampling of a wet deposition event that occurred in the western Algerian Basin, where we investigated the evolution of biogeochemical fluxes of both N and P and microbial activities.

140 2. Materials and Methods

2.1 Sampling strategy and measured parameters

The PEACETIME cruise (doi.org/10.17600/15000900) was conducted in the Mediterranean Sea, from May to June 2017, along a transect extending from the Western Basin to the center of the Ionian Sea (Fig. 1). For details on the cruise strategy, see Guieu et al. (2020). Short 145 duration stations (< 8 h, 10 stations named ST1 to ST10, Fig. 1) and long duration sites (5 days, 3 sites named TYR, ION and FAST) were occupied. Chemical composition of aerosols was quantified by continuous sampling along the whole transect. In addition, two rain events were sampled (Desboeufs et al., this issue, in prep.), one on the 29th of May at ION site, and a second one, a dust wet deposition event, at FAST site on the 5th of June.

150 At least 3 CTD casts were conducted at each short station. One cast focused on the epipelagic layer (0-250 m), another on the whole water column. Both of these were sampled with a standard, classical-CTD rosette equipped with ~~a sampling system~~ of 24 Niskin bottles (12 L), and a Sea-Bird SBE9 underwater unit ~~equipped~~ with pressure, temperature (SBE3), conductivity (SBE4), chlorophyll fluorescence (Chelsea Acquatracka) and oxygen (SBE43) 155 sensors. A third cast, from surface to bottom was ~~performed~~ under ‘trace metal clean conditions’ using ~~a second~~ instrumental package including a titanium rosette (called TMC-rosette) mounted on a Kevlar cable and equipped with Go-Flo bottles that were sampled in a dedicated clean lab container. The long duration sites were abbreviated as TYR (situated in the center of the Tyrrhenian Basin), ION (in the center of the Ionian Basin), FAST (in the 160 western Algerian Basin). These 3 sites were selected using satellite imagery, altimetry and Lagrangian diagnostics and forecasted rain events (Guieu et al., 2020). At these sites, repeated casts were performed over ~~a minimum of~~ 4 days; alternating CTD- and TMC- rosettes (Table 1). The succession of CTD casts at the FAST site is numbered in days relative to a rain event ~~collected~~ on board the ship. The first cast of the series was sampled 2.3 days before the rain

165 event, and the last 2 days after. The FAST site was revisited following the study of ST10 (3.8 days after the rain event).

Primary production (PP), prokaryotic heterotrophic production (BP), heterotrophic prokaryotic abundances (hprok), ectoenzymatic activities (leucine aminopeptidase (LAP) and alkaline phosphatase (AP)), were determined on water samples collected with the classical CTD-rosette. Dissolved inorganic nutrients, dissolved organic nitrogen (DON) and phosphorus (DOP) were measured on water samples collected using the TMC-rosette. LAP and AP were determined from two layers in the epipelagic waters (5 m depth and deep chlorophyll maximum (DCM)) at the short stations and at the ION and TYR sites In addition, LAP and AP were determined at 4 depths between 0 and 20 m for 4 profiles at FAST site, to 170 get insight on the variability within the ML.
175

2.2 Analytical methods and fluxes calculations

2.2.1 Nutrients in the atmosphere

For dry deposition estimations, the total suspended aerosol particles (TSP inlet) were 180 collected continuously throughout the campaign. Aerosol sampling was accomplished by using filtration units on adapted membranes for off-line chemical analysis (Tovar-Sanchez et al., 2020). In parallel to the total aerosol filter sampling, water soluble fractions of the aerosols was sampled continuously, using a Particle-into-Liquid-Sampler (PILS, Orsini et al., 2003). Moreover, two wet deposition events were sampled on board the ship during the 185 cruise, one at the ION site, one at the FAST site using rain collectors with on-line filtration (porosity 0.2 μ m) (details in Desbeoufs et al., this issue, in prep)

The nitrate and ammonium concentrations in the aerosols, abbreviated in the text to NO_3 and NH_4 respectively, (nitrite concentrations were under analytical detection limits) were 190 analyzed continuously on board from May 13th, using PILS sampling coupled on-line with double way ion chromatography (PILS-IC, Metrohm, model 850 Professional IC with Metrosep A Supp 7 column for anion measurements and Metrosep C4 column for cation measurements). The time resolution for PILS-IC analysis was 70 min. for anions and 32 min for cations. Dissolved Inorganic Nitrogen (DIN) fluxes released from the dry deposition were estimated by multiplying the NO_3 and NH_4 obtained by PILS-IC measurements by the dry settling velocities of N-bearing aerosols, i.e 0.21 and 1 cm s^{-1} for NH_4 and NO_3 , respectively (Kouvarakis et al., 2001). Mean concentrations were used from the PILS-IC data which were 195 measured (1) during the occupation at each short station lasting between 0.13 and 0.66 days

(i.e. enabling on average 5 measurements for NO₃ and 11 measurements for NH₄), and (2) between two successive casts at the sites with a time lag in between of 0.4 to 1.21 days (i.e. 200 enabling on average 15 measurements for NO₃ and about 30 for NH₄). At ST1, NH₄ and NO₃ concentrations were obtained using IC analyses following water extraction from aerosol filter sampling as the PILS-IC was not operational.

Total dissolved phosphate (TDP) concentrations were estimated from soluble P concentrations extracted from particulate aerosols collected on filters after ultrapure water 205 extraction HR-ICP-MS analysis (Neptune Plus, Thermo Scientific™) (Fu et al., this issue, in prep) since it was generally under detection limits using the PILS-IC technique. The frequency of TDP analysis was therefore less than for DIN: the filters sampled over the duration of the short station (0.28 -1.15 days depending on the stations). At the 3 sites, filters collected aerosols during periods including each CTD casts sampling date, when possible.

210 Atmospheric deposition flux of soluble P was estimated by multiplying the TDP concentration by a dry settling velocity of 1 cm s⁻¹. At the FAST site a 3 cm s⁻¹ velocity was used as this value is better adapted for lithogenic particles (Izquierdo et al., 2012). In the rain samples, collected onboard the ship, NO₃, NH₄ and dissolved inorganic phosphorus (DIP) were also determined using ion chromatography following recovery of the 215 dissolved fraction in the samples. The wet deposition fluxes of these nutrients were then estimated from the measured concentrations in the dissolved fractions from the rain samples, multiplied by total precipitation. Total precipitation was taken from the total hourly precipitation accumulated during the rain event over the region from the ERA5 hourly data reanalysis (Hersbach et al., 2018). Total precipitation was obtained by adding the hourly 220 rainfall onto the grid-points (0.25° x 0.25°) spanning the ship location, more or less 1° around this central grid-point for integrating the regional variability (Table 3). In the rain samples, total particulate P (TPP) and dissolved organic P (DOP) were also available. The dissolved fraction and solution from digestion (Heimburger et al., 2012) of particulate fractions in the filters were analysed by ICP-AES (Inductively Coupled Plasma Atomic Emission 225 Spectrometry, Spectro ARCOS Ametek®) for total particulate TPP. The speciation organic/inorganic of TDP was determined from ICP-MS and IC analysis. DOP was estimated from the difference between TDP, obtained by ICP-MS, and DIP, obtained by ion chromatography.

230 **2.2.2 Nutrients in the water column**

Seawater samples for standard nutrient analysis were filtered online ($< 0.2 \mu\text{m}$, Sartorius Sartobran-P-capsule with a $0.45 \mu\text{m}$ prefilter and a $0.2 \mu\text{m}$ final filter) directly from the GoFLo bottles (TMC-rosette). Samples collected in acid-washed polyethylene bottles were immediately analyzed on board. Micromolar nitrate + nitrite (NOx) and DIP were determined 235 using a segmented flow analyzer (AAIII HR SealAnalytical©) following Aminot and Kérouel (2007) with a limit of quantification of $0.050 \mu\text{M}$ for NOx and $0.020 \mu\text{M}$ for DIP. Samples for the determination of nanomolar concentrations of dissolved nutrients were collected in HDPE bottles previously cleaned with supra-pure HCl. For NOx (considered as NO3 as nitrite fraction was mostly negligible), samples were acidified to pH 1 inside the clean van and 240 analyzed back in the laboratory using a spectrometric method in the visible (540 nm), with a 1 m LWCC (Louis et al., 2015). The limit of detection was 6 nM , the limit of quantification was 9 nM and the reproducibility was 8.5%. DIP was analyzed immediately after sampling using 245 the LWCC method after Pulido-Villena et al. (2010), with a limit of detection of 1 nM (Pulido-Villena et al., 2021). Total dissolved phosphorus (TDP) and nitrogen (TDN) were measured using the segmented flow analyzer technique after high-temperature (120 °C) persulfate wet oxidation mineralization (Pujo-Pay and Raimbault, 1994). DOP (DON) was obtained as the difference between TDP (TDN) and DIP (NOx). Labile DOP (L-DOP) was determined as 31% DOP (Pulido-Villena et al., this issue, in prep.).
Total hydrolysable amino acids (TAAs) were determined as described in detail in Van 250 Wambeke et al. (2021). Briefly 1 ml of sample was hydrolyzed at 100°C for 20 h with 1 ml of 30% HCl and then neutralized by acid evaporation. Samples were analyzed by high performance liquid chromatography in duplicate according to Dittmar et al. (2009) protocols.

2.2.3 Biological stocks and fluxes in the epipelagic waters

Flow cytometry was used for the enumeration of autotrophic prokaryotic and eukaryotic cells, 255 heterotrophic prokaryotes (hprok) and heterotrophic nanoflagellates (HNF). Subsamples (4.5 mL) were fixed with glutaraldehyde grade I 25% (1% final concentration), flash frozen and stored at $-80 \text{ }^{\circ}\text{C}$ until analysis. Counts were performed on a FACSCanto II flow cytometer (Becton Dickinson). The separation of different autotrophic populations was based on their scattering and fluorescence signals according to Marie et al. (2000). For the enumeration of 260 hprok (Gasol and Del Giorgio, 2000), cells were stained with SYBR Green I (Invitrogen – Molecular Probes). HNF staining was performed with SYBR Green I as described in

Christaki et al. (2011). All cell abundances were determined from the flow rate, which was calculated with TruCount beads (BD biosciences).

265 Particulate primary production (PP) was determined at 6 layers from the shallow CTD casts (0-250 m) sampled before sun rise. Samples were inoculated with ^{14}C -bicarbonate and incubated in on-deck incubators ~~refrigerated using running~~ surface seawater and equipped with various blue screens to simulate different irradiance levels. After 24 h-incubations, samples were filtered through 0.2 polycarbonate filters and treated for liquid scintillation measurement as described in detail in Marañón et al. (2021). A temperature correction was applied as explained in Marañón et al. (2021). N_2 fixation rates (N2fix) were determined as described in Ridame et al. (2011) using 2.3 L of unfiltered seawater ~~(acid-washed polycarbonate bottles)~~ enriched with $^{15}\text{N}_2$ gas (99 atom% ^{15}N) to obtain a final enrichment of about 10 atom% excess. 24 h-incubations for N2fix were conducted under the same temperature and irradiance as the corresponding PP incubations.

270

275

To calculate heterotrophic prokaryotic production (BP) ~~epipelagic~~ layers (0-250 m) were incubated with tritiated leucine using the microcentrifuge technique as detailed in Van Wambeke et al. (2021). We used the empirical conversion factor of 1.5 ng C per pmol of incorporated leucine according to Kirchman (1993). ~~Indeed,~~ isotope dilution was negligible under these saturating concentrations as periodically checked with concentration kinetics. As we only used 2 on board temperature controlled dark-incubators, a temperature correction was applied as explained in Van Wambeke et al. (2021). Ectoenzymatic activities were measured fluorometrically, using the fluorogenic model substrates ~~that were~~ L-leucine-7-amido-4-methyl-coumarin (Leu-MCA) and 4-methylumbelliferyl-phosphate (MUF-P) to track 280 aminopeptidase (LAP), ~~activity~~ and alkaline phosphatase (AP), ~~activity~~ respectively, as described in Van Wambeke et al. (2021). Briefly, the release of MCA from Leu-MCA and MUF from MUF-P were followed by measuring the increase of fluorescence in the dark (exc/em 380/440 nm for MCA and 365/450 nm for MUF, wavelength width 5 nm) in a VARIOSCAN LUX microplate reader. Fluorogenic substrates were added at varying 285 concentrations in 2 ml wells (0.025, 0.05, 0.1, 0.25, 0.5 and 1 μM) in duplicate. ~~From the varying velocities obtained, we determined~~ the parameters V_m (maximum hydrolysis velocity) and K_m (Michaelis-Menten constant that reflects enzyme affinity for the substrate) as well as their corresponding errors by ~~fitting the data using~~ a non-linear regression using the 290 ~~following~~ equation:

$$V = V_m \times S / (K_m + S)$$

where V is the hydrolysis rate and S the fluorogenic substrate concentration added. ~~TAA and L-DOP were then used as substrates to determine LAP and AP *in situ* activities using Michaelis-Menten equations (Van Wambeke et al., 2021, Pulido-Villena et al., 2021.)~~

2.3. Vertical partition of the epipelagic layer

~~The ML can be in a state of stirring and the density and seawater properties are homogeneous, or in a state of rest with homogeneous density but it is the vertical variations in the non-conservative components (such as nutrients), dependent on momentum and heat fluxes at the interface with the atmosphere, that determine the strength and vertical extent of the mixing~~

305 ~~(Brainerd and Gregg, 1995). In this study, with the absence of concomitant turbulence measurements, the mixed layer depth (MLD) was estimated indirectly using the shape of CTD profiles. Classical methods to evaluate MLD from CTD profiles are based on thresholds of the vertical density gap (de Boyer Montegut et al., 2004; D'Ortenzio et al., 2005) or on the vertical extension of fixed buoyancy content (Moutin and Prieur, 2012). As discussed in~~

310 ~~Gardner et al. (1995), the choice of criterion is sensitive to the subtle changes from active mixing to rest, with consequences for the representative time scales of the MLD estimates. In this study, the ML was shallow (10 - 20 m), rapidly activated by the mechanical effects of the wind, and sampled at high frequency (some hours at long duration stations). An approach based on buoyancy criterion has been preferred to resolve short term fluctuations in the~~

315 ~~mixing state, and MLD was determined as the depth where the residual mass content is equal to 1 kg m^{-2} , with an error of estimation of 0.5 m relative to the vertical resolution of the profile (1 m).~~

In the ~~current case of a shallow ML in such a LNLC system, the nutrient depleted layer comprises the ML and the layer below, referred to hereafter as 'NDLb' (b for bottom or base) when examining the NO_3 distribution and as PDLb when considering the DIP distributions.~~ This layer vertically extends between the MLD and the nitracline (phosphacline) depth (Fig. 2). The latter interface is estimated by the depth of ~~the~~ NO_3 (DIP) depletion density, which is the deepest isopycnal at which micromolar NO_3 (DIP) is zero (Kamykowski and Zentara, 1985; Omand and Mahadevan, 2015). The NO_3 (DIP) depletion density is estimated at every 325 discrete profile of micromolar NO_3 (DIP) concentration by the intercept of the regression line reported in a nutrient-density diagram.

There are various mechanisms, dynamical or biological, that can trigger exchanges of nutrients between the ML and NDLb (PDLb). Using the hypothesis of vertical (one-dimensional) regimes, there are two processes of exchange, by diffusion or advection (Du et al., 2017). The flux of nutrient can be expressed as:

$$F_{NO_3} = F_{DIF} + F_{ADV}$$

The diffusive flux F_{DIF} is expressed by the gradient of nutrient concentration times a vertical diffusivity coefficient K_z as:

$$F_{DIF} = K_z \times (NO_3_{ML} - NO_3_{NDLb}) / MLD$$

335 The typical magnitude of K_z in the surface layers of the PEACETIME stations is assessed to be $10^{-5} \text{ m}^2 \text{ s}^{-1}$, as discussed in Taillardier et al. (2020).

The advective flux F_{ADV} corresponds either to the entrainment of deeper water in the mixed layer due to erosion of the near-surface pycnocline, or to the detrainment of waters below the mixed layer by restratification, depending on the variations in wind stresses and solar heating
340 (Cullen et al., 2002). It is expressed as the variation in the nutrient concentration across the ML times the temporal variation of the MLD, as:

$$F_{ADV} = (NO_3_{ML} - NO_3_{NDLb}) \times dMLD / dt$$

A shallow ML (10 - 20 m) is primarily influenced by wind bursts that lead to intermittent variations of several meters per day (10^{-5} m s^{-1}) in the MLD. These advective fluxes provide
345 transient exchanges that are one order of magnitude greater than well-established diffusive fluxes. As a consequence, over the time scale of a significant atmospheric deposition, and the associated rapid variations of the MLD, the input of atmospheric nutrients would preferentially be exported below the ML by advection rather than by diffusion. In other terms, using the hypothesis of non-stationary regimes due to rapid changes in atmospheric conditions
350 (that control both the mixing state of the interface and atmospheric nutrient inputs), we assume that vertical advection is the main process of exchange.

At the short stations and sites, the term $NO_3_{ML} - NO_3_{NDLb}$ can be inferred by the difference between mean nanomolar (LWCC) concentrations inside the NDLb and the mean inside the ML. Since advective flux estimates require knowledge of the evolution of the MLD over time,
355 such fluxes are only accessible at the sites. At short stations, as advective fluxes could not be characterized, only a qualitative assessment of nutrient fluxes across ML is given. When $NO_3_{ML} - NO_3_{NDLb} < 0$, the NDLb is supplied with nutrients across the nutricline, and could be then possibly transferred into the ML. This means that nutrients within the ML are impacted by inputs from below. When $NO_3_{ML} - NO_3_{NDLb} > 0$, the ML is supplied in nutrients

360 from the atmosphere which are further exported into the NDLb. Vertical distributions of DIP, along the longitudinal transect, are described in detail in a companion paper (Pulido-Villena et al., 2021). In this study, we will focus on phosphate exchanges between the ML and PDLb and relationships with NO₃ distribution only at the high-frequency sampled FAST site.

365 **2.4 Budget from the metabolic fluxes**

Trapezoidal integration was used to integrate BP, PP and N₂fix within the ML. The biological activity at the surface was considered to be equal to that of the first layer sampled (around 5 m depth at the short stations, 1 m depth at the FAST site). When the MLD was not sampled, the volumetric activity at this depth was linearly interpolated between the 2 closest data points
370 above and below the MLD.

We used an approach similar to Hoppe et al. (1993) to compute the *in situ* hydrolysis rates for LAP and AP. We assumed that total amino acids (TAA) could be representative of dissolved proteins. *In situ* hydrolysis rates of LAP and AP were determined using molar concentrations of TAA and L-DOP, respectively and used as the substrate concentration in the Michaelis-
375 Menten kinetics. For LAP, the transformation of *in situ* rates expressed in nmol TAA hydrolyzed L⁻¹ h⁻¹ were then transformed into nitrogen units using N per mole TAA, as the molar distributions of TAA were available. Integrated *in situ* LAP hydrolysis rates were calculated assuming the Michaelis-Menten parameters V_m and K_m obtained at a 5 m depth to be representative of the whole ML. Thus an average *in situ* volumetric LAP flux in the ML
380 was obtained by combining the average TAA concentrations in the ML with these kinetic parameters, and multiplying this volumetric rate by the MLD. Daily BP, AP and LAP integrated activities were calculated from hourly rates x 24. Assuming no direct excretion of either nitrogen or phosphorus, the quota C/N and C/P of cell demand is equivalent to the cell biomass quotas. We used molar C/N ratios derived from Moreno and Martiny (2018) (range
385 6-8, mean 7) for phytoplankton and from Nagata et al. (1986) for heterotrophic prokaryotes (range 6.2-8.4, mean 7.3). C/P of sorted cells (cyanobacteria, picophytoeukaryotes) in P depleted conditions ranged from 107 to 161 (Martiny et al., 2013), and we considered a mean of 130 for phytoplankton. A value of 100 was used for heterotrophic prokaryotes (Godwin and Cotner, 2015).

390

3. Results

3.1 Nutrient patterns and biological fluxes along the PEACETIME transect

The ML ranged between 7 m at ST9 and 21 m at ST1 (Table S1, Fig. 3). The nitracline was
395 shallow in the Provençal Basin (50 – 60 m), dropping to 70 m in the Eastern Algerian and
Tyrrhenian Seas; becoming deeper in the Western Algerian and Ionian Seas (80 - 90 m, Table
S1). Mean NO₃ concentrations in the NDLb ranged from the quantification limit (9 nM) to
116 nM (Table S1, Fig. 4). In the ML, mean NO₃ concentrations ranged from 9 to 135 nM.
For the ‘group 1’ stations (see Table S1), the NO₃ concentrations were low (below 50 nM)
400 within both the ML and the NDLb, with weak differences precluding any gradient between
the two layers. For the ‘group 2’ stations, NO₃ concentrations were moderate (50 - 80 nM)
both within the ML and the NDLb but still exhibiting a small difference between the two
layers, indicating again no significant instantaneous exchanges. For ‘group 3’, higher NO₃
concentrations were measured in both the ML and the NDLb (> 80 nM) but the small positive
405 differences (< 20 nM) between the two layers still indicate weak or negligible exchanges
between the two layers. For ‘group 4’, high and moderate NO₃ concentrations were measured
within the ML and NDLb, respectively, with a large positive difference (> 20 nM) between
the layers. This indicates the presence of a gradient from the ML to the NDLb.

At 5 m depth, V_mLAP ranged from 0.21 to 0.56 nmol MCA-leu hydrolyzed l⁻¹ h⁻¹, and K_m
410 LAP ranged from 0.12 to 1.29 μ M. The mean TAA within the ML ranged from 0.17 to 0.28
 μ M. From these 3 series of parameters, we derived the mean *in situ* LAP hydrolysis rate
within the ML, which ranged from 0.07 to 0.29 nmol N l⁻¹ h⁻¹ (results not shown but detailed
in Van Wambeke et al., 2021).

The vertical distribution of PP and BP for the short stations are described in Marañon et al.
415 (2021). Briefly, PP exhibited a deep maximum close to the DCM depth or slightly above
whereas vertical distribution of BP generally showed 2 maxima, one within the mixed layer,
and a second close to the DCM. Integrated PP (Table 1, Table S2) ranged from 138 (TYR17
May) to 284 (SD1) mg C m⁻² d⁻¹. Integrated BP (0-200 m) ranged from 44 (ION27may) to
113 (FAST+0.53) mg C m⁻² d⁻¹. Overall, in absence of a rain event the Mediterranean Sea, at
420 the time of the PEACETIME cruise, the transect exhibited the classical west-east gradient of
increasing oligotrophy detected by ocean colour (see Fig. 8 in Guieu et al., 2020),

3.2 N budgets and fluxes at short stations

Biological rates (all expressed in N units) within the ML at the short stations were compared.
425 (Table 2). Phytoplankton N demand (phytoN demand) was the greatest rate, followed by

heterotrophic prokaryotic N demand (hprokN demand). On average, phytoN demand was 2.9 times greater than that of hprokN, but with a large variability (min x1.5, max x8.1). LAP hydrolysis rates represented between 14 and 66 % of the hprokN demand (mean \pm sd : 37% \pm 19%), N₂ fixation rates represented between 1 to 4.5% of the phytoN demand (2.6% \pm 1.3%) 430 and 3 to 11% of the hprok N demand (6.4% \pm 2.4%). N₂ fixation rates integrated over the ML correlated slightly better with hprokN demand ($r = 0.75$) than with phytoN demand ($r = 0.66$). Dissolved inorganic N (DIN=NO₃+NH₄) solubilized from dry atmospheric deposition ranged from 17 to 40 $\mu\text{mol N m}^{-2} \text{d}^{-1}$ with on average 79% of this being NO₃ (Table 2). This new DIN input was similar or higher than N₂ fixation rates within the ML (from x1.3 to x11, 435 mean x 4.8-fold). On average within the ML, the new DIN from dry deposition represented 27% of the hprokN demand (range 10-82%) and 11% of the phytoN demand (range 1-30%).

3.3 Biogeochemical evolution at the ION site

440 The ION site was occupied from the 25th to the 29th of May. Rain events in the vicinity of the ship were observed on May 26th and May 29th (Desboeufs et al., this issue, in prep). On the 29th of May the rain event was associated with a rain front covering more than 5 000 km². A rain sample could be taken on board between 5:08 and 6:00 (local time), i.e. just 3 hours before the last CTD cast. The chemical composition of the rain indicated an anthropogenic 445 background influence (Desboeufs et al., this issue, in prep.).

TDP solubilized from dry atmospheric deposition decreased from 268 nmol P m⁻² d⁻¹ May 25th -26th to 124 nmol P m⁻² d⁻¹ May 27th-28th). DIN fluxes from dry atmospheric deposition were on average 29 \pm 4 $\mu\text{mol N m}^{-2} \text{d}^{-1}$ with no significant difference during the occupation of the site (Table S2). In the rain, the molar ratio DIN/DIP was 208. DOP in the collected rain 450 was also an important source (60%) of the total dissolved P from that wet deposition (Table 3).

CTD casts, dedicated to biogeochemical studies, were taken each 24 h for biological fluxes or 48 h for DIP and NO₃. Thus the time sequence for nutrients in the water column at ION is given for only by three profiles. The first profile (25th of May before rain events in the area) is 455 'flat', corresponding to fair weather conditions and a shallow ML with low and homogeneous concentrations of NO₃ in the ML and the NDLb (Fig. 4). Shortly after, there was an atmospheric depression some events of rain were observed in the area on May 26th but not on board, and the ML started to deepen 13 h before the second cast sampling nutrients (on the

27th of May). This cast was marked by high nitrate in the ML (Fig. 3). The mixing should
460 have set up a homogeneous ML, but wind conditions rose to 20 kt just at the time of the cast
(Fig. 3). The interval between the second and the third cast sampling nutrients (29th of May,
cast done 3 hours after the rain sampled on board) is marked by a slight relaxation of weather
depression, and a deepening of the ML down to 20 m. This cast was marked by a NO₃
decrease in both the ML and NDLb, but values were higher in ML. Given the remaining
465 signature at 15 m and the deepening of the ML, the two layers might have stayed isolated.
However, the calculation of vertical advective fluxes between the layers showed a downward
flux in the first interval 25-27 May (Fig. 4, Table S1) and an upward flux in the second
interval (27-29 May).

Due to the lack of high frequency sampling, it was also particularly difficult to assess the
470 direct time evolution effects of dry atmospheric deposition at the ION site. Nevertheless, it
was clear from the casts sampled on the 27th and 29th of May that this site was characteristic
of group 4 (i.e. higher NO₃ concentrations in the ML than in the NDLb), indicating recent
inputs from the atmosphere. Ectoenzymatic activities were only sampled on the 25th of May.
Vm of LAP at 5 m (0.22 nmol N l⁻¹ h⁻¹) was one of the lowest values recorded during the
475 cruise whilst Vm of AP showed the highest value (5.6 nmol P l⁻¹ h⁻¹). PP integrated over the
euphotic zone increased slightly from 188 to 226 mg C m⁻² d⁻¹ (Table S2), but due to changes
in the MLD at the ION site (range 11-21 m) this trend was not visible when integrating PP
over the ML. Integrated over the ML, BP increased slightly, from 7.5 to 10.3 mg C m⁻² d⁻¹
between the 25th and the 29th of May, and indicated that hprok benefited more from the
480 atmospheric inputs than the autotrophs as PP decreased at 5m depth (Fig. S1, Table S2). The
profiles of hprok and *Synechococcus* abundances showed no particular trend with time, with
higher variations within the DCM (Fig. S1).

3.4 N budgets and fluxes at the FAST site

485 During the time at the FAST site, two periods of rains occurred: the evening of June 2nd-3rd
and the early morning of the 5th (Tovar-Sanchez et al., 2020). On a spatial scale, the rain
radar data indicated the presence of a rain front with patchy, numerous and intense rain events
occurring over a large area surrounding the ship's location. These two episodes were
concomitant with a dust plume transported in altitude (between 1 and 4 km) and resulted in
490 wet deposition of dust (Desboeufs et al., this issue, in prep.). The second rain event was
sampled on board on June 5th (between 02:36 and 03:04, local time) and was associated with

a dust wet deposition flux $\sim 40 \text{ mg m}^{-2}$. The DIN/DIP ratio in the rain reached 480 (Table 3). After the rain, daily fluxes of DIN solubilized from dry aerosol deposition strongly decreased from 45 to $9.8 \text{ } \mu\text{mol N m}^{-2} \text{ d}^{-1}$ between June 4th and 5th.

495

The beginning of the sampling at FAST site (-2.3; -1.5; -0.25) was marked by moderate and similar decreases in NO₃ concentration within the ML and NDLb. Integrated stocks of NO₃ within the ML (Table S2) reflected slight changes with MLD (from 14 to 10 m during this time interval).

500 On June 5th, the rain event (Table 3) was associated with a strong wind burst and an abrupt mixing. The comparison between NO₃ concentrations from two casts, sampled 6 h before and 6 h after the rain, (FAST-0.25 and FAST+0.24), showed a clear N enrichment of the ML as mean NO₃ increased from 56 to 93 nM and NO₃ integrated stocks increased by $888 \text{ } \mu\text{mol N m}^{-2}$ (Fig. 3, Table S2). There was also clear difference in the mean NO₃ concentrations 505 between ML and NDLb (93 ± 15 vs 51 ± 7 nM, respectively). This is the highest NO₃ difference observed during the cruise between these 2 layers (Fig. 4), confirming that this ML enrichment could not be attributed to inputs from below. The relaxation of this wind burst was progressive, with a continuous deepening of the ML (Table S1). The export of the atmospheric NO₃ into the NDLb was maximal after the rain event (FAST+0.24). At the end 510 of the site occupation period (FAST+3.8) high NO₃ concentrations (mean 135 nM) were measured again within the ML.

DIP concentration dynamics were different from NO₃ with the DIP integrated fluxes within the ML similar 6 h before and 6 h after the rain ($136 \text{ } \mu\text{mol m}^{-2}$). It is only from then on, that DIP flux progressively increased reaching a maximum ($281 \text{ } \mu\text{mol P m}^{-2}$) one day after the rain 515 (FAST+1).

Immediately after the rain, integrated PP (euphotic zone) decreased from $274 \text{ mg C m}^{-2} \text{ d}^{-1}$ (FAST-0.9) to $164 \text{ mg C m}^{-2} \text{ d}^{-1}$ (FAST+0.07) and continued to decrease the following day. It is only 3.8 days after the rain that the initial values (before the rain) of integrated PP could be observed again (Table S2). Such variations were mostly due to changes in volumetric rates 520 within the DCM depth (Fig. S2), as the activity did not change significantly within the ML ($28\text{--}33 \text{ mg C m}^{-2} \text{ d}^{-1}$, Fig. S2, Fig. 5). Integrated BP over 0-200 m showed the opposite trend to that of PP and tended to increase after the rain (from $86 \pm 3 \text{ mg C m}^{-2} \text{ d}^{-1}$ ($n = 4$) before, and up to $113 \text{ mg C m}^{-2} \text{ d}^{-1}$ (FAST+0.5) after (Table S2)). Although modest, this increasing trend was also visible when integrating BP only over the ML (12-15 before; 15-19 $\text{mg C m}^{-2} \text{ d}^{-1}$

525 after). The abundances of picophytoplankton groups were mostly varying in the vicinity of the DCM depth with peaks occurring 1-2 days after the rain (grey profiles, Fig S3), in particular for prokaryotes (*Prochlorococcus*, *Synechococcus*). Heterotrophic prokaryotes and nanoflagellate abundances slightly increased within the DCM depth after the rain.

530 **4. Discussion**

The specific context of the oceanographic survey constrained the data analysis: biogeochemical responses to a rain event have been scaled in time over a few days (3 - 5), and in space spanning tens of km (40 - 50). Their evolution was restricted to the vertical 535 dimension, integrating lateral exchanges by horizontal diffusion or local advection that occurred over the prescribed space and time scales. In the vertical dimension, exchanges of nutrients across the ML were controlled by advection due to rapidly changing conditions (MLD fluctuations along with nutrient inputs from the atmosphere) rather than to diffusion between stationary pools. Four groups of stations, corresponding to different stages of ML 540 enrichment and relaxation, due to the nutrient inputs from single rain events, have been characterized based on the differences in NO₃ concentration between ML and NDLb (see section 2.4). As shown in Fig. 4, this succession of stages is in agreement with the NO₃ fluxes from above and below the ML. Moreover, they provide a temporal scaling of the oceanic response to atmospheric deposition, with a quasi-instantaneous change at the time of the rain 545 event and a 2-day relaxation period to recover to pre-event conditions

In this context, we will i) discuss the nitrogen budget within the ML at the short stations considered as a ‘snapshot’, and ii) analyze in detail, using a time series of CTD casts, the biogeochemical changes within the ML and the NDLb following the atmospheric wet deposition event at the FAST site, discussing the possible modes of transfer of nutrients 550 between these 2 layers.

4.1 A snapshot of biological fluxes in the ML and their link to new DIN from atmospheric dry deposition

The dependence of hprok on nutrients rather than on labile organic carbon during 555 stratification conditions is not uncommon in the MS (Van Wambeke et al., 2002, Céa et al., 2017; Sala et al., 2002) and has also been shown during PEACETIME cruise (P, or N,P colimitation, Fig. S4). Hprok have an advantage due to their small cell size and their kinetic

systems which are adapted to low concentration ranges of nutrients (for example for DIP see Talarmin et al., 2015). Under such conditions of limitation, hprok will react rapidly to new 560 phosphorus and nitrogen inputs, coming from atmospheric deposition. During an artificial *in situ* DIP enrichment experiment in the Eastern Mediterranean, P rapidly circulated through hprok and heterotrophic ciliates, while the phytoplankton was not directly linked to this ‘bypass’ process (Thingstad et al., 2005). Bioassays conducted in the tropical Atlantic Ocean have also shown that hprok respond more strongly than phytoplankton to nutrients from 565 Saharan aerosols (Marañón et al. 2010), a pattern that has been confirmed in a meta-analysis of *in vitro* dust addition experiments (Guieu and Ridame, in press; Gazeau et al., 2021).

We considered hprokN demand together with phytoN demand and compared it to 570 autochthonous (DON breakdown by ectoenzymatic activity) and allochthonous (atmospheric deposition) sources. To the best of our knowledge this is the first time that these fluxes are compared based on their simultaneous measurements at sea. A high variability was observed between the 10 short stations (Table 2). The regeneration of nitrogen through aminopeptidase activity was clearly the primary provider of N to hprok as 14 to 66% (mean \pm sd : 37% \pm 19%) of the hprokN demand could be satisfied by *in situ* LAP activity. Such percentages may 575 be largely biased by the conversion factors from C to N and propagation of errors for the LAP hydrolysis rates and BP rates. However, the C/N ratio of hprok is relatively narrow under large variations of P or N limitation (6.2 to 8.4; Nagata, 1986).

Other regeneration sources exist such as direct excretion of NH4 or low molecular weight 580 DON sources with no necessity for hydrolysis prior to uptake (Jumars et al., 1989). For instance, Feliú et al. (2020) calculated that NH4 and DIP excretion by zooplankton would satisfy 25-43% of the phytoN demand and 22-37% of the phytoP demand over the whole euphotic zone. Such percentages suggest that direct excretion by zooplankton along with ectoenzymatic activity, provide substantial N for biological activity.

N₂ fixation is also a source of new N that can directly fuel hprok as some diazotrophs are 585 heterotrophic (Delmont et al. 2018, and references therein), or indirectly, as part of the fixed N₂ that rapidly cycles through hprok (Caffin et al., 2018). Furthermore, it has been observed that there is a better coupling of N₂fix rates with BP rather than with PP in the eastern MS (Rahav et al., 2013b). This was also observed within the ML in this study. Our data show that the hypothetical contribution of N₂fix rates to hprokN demand within the ML was low (6.4 \pm 590 2.4%) and consistent with the low N₂fix rates observed in the MS (i.e Rahav et al., 2013a;

Ibello et al., 2010; Ridame et al., 2011; Bonnet et al., 2011). This differs from other parts of the ocean primarily limited by N but not P, such as the south eastern Pacific where N₂ fixation rates are high (Bonnet et al., 2017) and can represent up to 81 % of the hprokN demand (Van Wambeke et al., 2018).

595 Considering LAP as the most relevant regeneration source of N, it is clear that even the sum of LAP activity and N₂ fixation were not sufficient to meet hprokN demand (cumulated, these fluxes contributed 19 to 73% of HbactN demand). The last source of new N we examined was DIN released by dry atmospheric deposition. Such DIN fluxes presented a low variability along the transect ($29 \pm 7 \text{ } \mu\text{mol N m}^{-2} \text{ d}^{-1}$ at the short stations) and were among the lowest measured in the Mediterranean environment, which normally ranges from 38 to 240 $\mu\text{mol N m}^{-2} \text{ d}^{-1}$ (Desboeufs et al., in press). It has to be noted that the fluxes measured during the PEACETIME cruise are representative of the open sea atmosphere while published fluxes were measured at coastal sites where local/regional contamination contributes significantly to the flux (Desboeufs, in press). Atmospheric deposition also delivers organic matter (Djaoudi et al., 2017, Kanakidou et al., 2018), which is bioavailable for marine hprok (Djaoudi et al., 2020). Dissolved organic nitrogen (DON) released from aerosols, not determined here, can be estimated from previous studies. DON solubilized from aerosols contributes 19 to 42% of the total dissolved N released from dry deposition in the MS (Desboeufs, in press), with an average of 32%. Considering this mean, DON released from dry deposition was estimated to 600 range from 8 to 19 $\mu\text{mol N m}^{-2} \text{ d}^{-1}$ at the short duration stations. The total dissolved N solubilized from dry deposition (inorganic measured + organic estimated) would thus represent 14 to 121% of the hprokN demand. Because of the low variability in DIN (and estimated DON) fluxes derived from dry deposition, the atmospheric contribution was mainly driven by biogeochemical conditions and not by the variability of atmospheric fluxes during 605 the cruise (CV of Nprok N demand and phyto N demand at the short stations were 45% and 89%, respectively, and that of DIN flux 25%). However, the calculated contribution can also be biased by the deposition velocity used to calculate DIN solubilized from the dry deposition. Deposition velocity was set at 1 cm sec⁻¹ for NO₃ and 0.21 cm sec⁻¹ for NH₄. As NO₃ was the dominant inorganic form released by dry deposition, it is clear that the choice of 610 1 cm sec⁻¹ for NO₃ influenced its contribution. This choice was conditioned by the predominance of NO₃ in the large mode of Mediterranean aerosols such as dust or sea salt particles (e.g., Bardouki et al., 2003). However, the deposition velocity of NO₃ between fine and large particles could range from 0.6 to 2 cm sec⁻¹ in the Mediterranean aerosols (e.g., 615 620

625 Sandroni et al., 2007). Even considering the lower value of 0.6 cm sec⁻¹ from the literature, the contribution of DIN from atmospheric dry deposition to hprokN demand within the ML would still be significant (up to 72%).

4.2 Biogeochemical response after a wet event – N and P budgets at FAST site

630 Rain events are more erratic than dry atmospheric deposition but represent on average much higher new nutrient fluxes to the MS surface waters on an annual basis, e.g. 84% of annual atmospheric DIN fluxes in Corsica Island (Desboeufs et al., 2018). On the scale of the 635 Mediterranean basin, the annual wet deposition of DIN was found to be 2-8 times higher than DIN from dry deposition (Markaki et al., 2010). Wet deposition also contributes significantly to DON atmospheric fluxes in the MS: For example at Frioul Island (Bay of Marseille, NW MS), total (wet + dry) DON atmospheric fluxes ranged between 7 and 367 $\mu\text{mol DON m}^{-2}$ day⁻¹ and represented $41 \pm 14\%$ of the total atmospheric nitrogen flux (Djaoudi et al., 2018). In the Eastern MS (Lampedusa Island) DON atmospheric fluxes ranged between 1.5 and 250 $\mu\text{mol DON m}^{-2}$ day⁻¹ contributing to 25% of the total atmospheric nitrogen flux, respectively (Galletti et al., 2020). In both studies, bulk atmospheric fluxes of DON were positively 640 correlated with precipitation rates, indicating the preponderance of wet deposition over dry deposition.

645 At the FAST site, the maximum net variations of NO₃ and DIP concentrations within the ML before/after the rainy period reached $1520-665 = +855 \mu\text{mol N m}^{-2}$ for NO₃ and $281-137 = +144 \mu\text{mol P m}^{-2}$ for DIP (Table S2). In other terms, based on a mean MLD of 16 m, the net observed increases in the ML were + 9 nM DIP and + 54 nM NO₃. As the rain event in the area would have increase by 0.07 nM DIP and 21 nM NO₃ concentrations over the whole mixed layer, the net variations observed in the ML are thus higher than the calculated variation in stocks deduced from the N and P concentrations of this rain event (Table 3). This 650 is still true when including all P or N chemical forms (particulate and soluble inorganic + organic fractions). For example the P concentration in the ML would increase by ~0.68 nM. As described in the results section 3.4, the rains affecting the FAST site were spatially patchy over a large area (~40-50 km radius around the R/V). Thus, we could consider that the biogeochemical impacts observed at FAST site were probably due to a suite of atmospheric 655 events rather than due to the single event collected on board. It is possible that meso- and sub-

mesoscale dynamics encountered at FAST site (Figs 5 and 12 in Guieu et al., 2020) can explain such cumulative impact.

Interestingly, a delay of about 19 h was observed in the maximum net accumulation within the ML between DIP (FAST+1.05) and NO₃ (FAST+0.24). The DIN/DIP ratio in the rain (1438) was much higher than the Redfield ratio. As the biological turnover of DIP in the MS is rapid (from min to few h, Talarmin et al., 2015), new DIP from rain might have behaved differently than DIN. Two different mechanisms can explain this delay: (i) processes linked to bypasses and luxury DIP uptake (storage of surplus P in hprok before a rapid development of grazers (Flaten et al, 2005; Herut et al 2005, Thingstad et al., 2005) that are later responsible for DIP regeneration) so that DIP net accumulation is delayed and/or (ii) abiotic processes such as rapid desorption from large sinking particles followed by adsorption of DIP onto submicronic iron oxides still in suspension as observed experimentally in Louis et al. (2015). The first proposed mechanism may be supported by the observed increase of BP, along with a stable PP which suggests an immediate benefit of the new nutrients from rain by hprok rather than phytoplankton. The so-called luxury DIP uptake by the competing organisms like hprok is efficient (small cells with high surface/volume ratio and DIP kinetic uptake adapted to low concentrations). It is of course difficult to quantify such *in situ* variations in comparison to mesocosms/minicosms dust addition experiments, in which clearly heterotrophy is favoured first (Marañón et al., 2010; Guieu et al., 2014b; Gazeau et al., 2021). Few attempts in the field have confirmed these trends (Herut et al., 2005, Pulido-Villena et al., 2008) but, as stated in the introduction, these studies lacked high frequency sampling.

The second proposed mechanism, the abiotic desorption/adsorption, is compatible with the observed 19 h delay (Louis et al., 2015). Note that most of the estimates of such abiotic processes are from dust addition experiments with contrasting results, some showing this abiotic process of absorption/desorption while the particles are sinking (Louis et al., 2015), and other not (Carbo et al., 2005) or showing it as negligible in batch experiments (Ridame et al., 2003). It is possible that DIP adsorbed onto large particles rapidly sinks out of the ML, and desorbs partly during its transit in the PDLb, where it could stay longer thanks to the pycnoclines barriers.

We tentatively made a P budget between FAST+1.05 and FAST+2.11 where a net decrease of DIP (-87 $\mu\text{mol P m}^{-2}$) was observed in the ML. During this time, advective flux of DIP toward the PDLb was not detectable as DIP concentrations within the ML were always lower than within the PDLb (Pulido-Villena et al., 2021.). This indicated that the DIP was assimilated

and/or transformed to DOP via biological processes, and/or adsorbed onto particles and then
690 exported to PDLb by sedimentation. By integration of PP and BP over this period (34.5 and
19.7 mg C m⁻², respectively) and, by assuming that all the disappearing 87 µmol DIP m⁻²
would be consumed by hprok and phytoplankton, we could estimate a C/P ratio reached in
their biomass of ((34.5+19.7)/12x1000)/87=52. Such C/P suggests that DIP was not limiting
these organisms anymore. Indeed a decrease of C/P quotas may highlight a switch from P to
695 C limitation for heterotrophic bacteria (Godwin and Cotner, 2015) and from P to N limitation
or increased growth rates for phytoplankton (Moreno and Martiny, 2018). Furthermore, as
DIP is also recycled via alkaline phosphatase within the ML, we also consider another source
of DIP via alkaline phosphatase activity, from which *in situ* activity (see Van Wambeke et al.,
2021 for *in situ* estimates) could release 139 µmol DIP m⁻² during this period. Assuming also
700 that DIP resulting from of AP hydrolysis was fully assimilated for P biological needs, then
C/P ratio would be (((34.5+19.7)/12x1000))/(87+139)=19. This low ratio seems unrealistic
for phytoplankton (Moreno and Martigny, 2018) as well as hprok, even growing in surplus C
conditions (Makino et al., 2003; Lovdal et al., 2008; Godwin and Cotner, 2015).
Some of the P recycled or brought into the ML from atmospheric deposition has consequently
705 been exported below the ML. DIP is abiotically adsorbed on mineral dust particles (Louis et
al., 2015), most of them sinking, and thus constitute a source of export out of the ML. It is
also possible that such sorbing process on dust particles enables the export of other P-
containing organic molecules, for instance DOP or viruses produced following luxury DIP
assimilation. Free viruses, richer in P than N relative to Hprok, could adsorb, like DOM, onto
710 dust particles and constitute a P export source. Indeed, free viruses sorb onto black carbon
particles, possibly reducing viral infection (Mari et al., 2019; Malits et al., 2015). However,
particle quality is a determining factor for DOM or microbial attachment, and what has been
shown for black carbon particles is not necessarily true for dust particles. For instance the
addition of Saharan dust to marine coastal waters led to a negligible sorption of viruses to
715 particles and increased abundance of free viruses (Pulido-Villena et al., 2014), possibly linked
to an enhancement of lytic cycles in the ML after relieving limitation (Pradeep Ram and
Sime-Ngando, 2010).

We are aware of all the assumptions made here ((i) conversion factors, (ii) *in situ* estimates of
alkaline phosphatase, (iii) some missing DIP sources in the budget, such as the excretion of
720 zooplankton estimated to amount to 22-37% of the phytoP demand at FAST site (Feliú et al.,
2020), iv) lack of knowledge on the different mechanisms linking P to dust particles, and (iv)

the hypothesis which considers the station as a 1D system. Nevertheless, all these results together suggest that both luxury consumption by Hprok and export via scavenging on mineral particles probably occurred simultaneously and could explain the observed variations of DIP in the ML.

725

For NO₃, and in contrast to the observations for DIP, we observed physical exchanges by advection between the ML and NDLb. A N budget within the ML during the period of net NO₃ decrease (between FAST+0.24, and FAST+2.11, Table S2), indicates a net loss of 1343 730 $\mu\text{mol N m}^{-2}$ within the ML. For this period lasting 1.8 days, the time-integrated phytoN and hprokN demands were 682 $\mu\text{mol N m}^{-2}$ and 378 $\mu\text{mol N m}^{-2}$, respectively, so that total biological demand in the ML was 1060 $\mu\text{mol N m}^{-2}$. During this period, the possible N sources used were disappearing stocks of NO₃ (net diminution assumed to be consumption = 1343 $\mu\text{mol N m}^{-2}$), as well as N₂ fixation and *in situ* aminopeptidase activity where fluxes 735 integrated over this time period were 13 and 87 $\mu\text{mol N m}^{-2}$, respectively. In total, the possible source of N amounted to 1443 $\mu\text{mol N m}^{-2}$. Keeping in mind that the same potential caveats pointed to DIP (see above) also apply for the calculation of N budget, the biological N demand appeared lower than the sources (difference ~380 $\mu\text{mol N m}^{-2}$). On the other hand, at FAST site, vertical advective fluxes of NO₃ from ML to NDLb were up to 337 $\mu\text{mol N m}^{-2} \text{ d}^{-1}$ 740 (Fig. 4), i.e. ~600 $\mu\text{mol N m}^{-2}$ was lost from the ML over 1.8 days. From these two different approaches, exported NO₃ should range between 380 and 600 $\mu\text{mol N m}^{-2}$ over this period. Thus, about 40% of the NO₃ accumulated in the ML after the rain was likely exported by vertical advection to the NDLb. Organisms present in the DCM could benefit of this input of new nutrients. Indeed, PP and abundances of all 4 phytoplankton groups (*Synechococcus*, 745 *Prochlorococcus*, nano and picoeukaryotes) increased at the DCM after 24h and remained high for 2 days after the rain event (Fig. S3). The increase in abundances were higher for prokaryotic phytoplankton abundances, as such organisms would likely benefit from their small size and their ability to use DON/DOP organic molecules (Yelton et al., 2016).

750

5. Conclusions

This study reports for the first time, in the context of an oceanographic cruise, simultaneous sampling of atmospheric and ocean biogeochemical parameters to characterize *in situ* the biogeochemical responses to atmospheric deposition within the ML. High-frequency sampling, in particular at the FAST site, confirmed the transitory state of exchanges between

755 the ML and the NDLb. Even if dry deposition measured along the transect was homogeneous and amongst the lowest observed in the MS, that input could represent up to 121% of the hprokN demand. Furthermore, the signature of the dust wet deposition event on DIP and DIN concentrations was clearly emphasized, considering both the local rain fluxes and the horizontal oceanic mixing of water masses affected by the rain front. Finally, a comparison
760 with the mesocosms results (where the fertilization is more important due to high dust concentrations) is hard to extrapolate with the data presented here.

Our results have shown the important role played by the ML in the biogeochemical and physical processes responsible for transfers of matter and nutrients between the atmosphere and the nutrient depleted layer below. Thanks to the use of the LWCC technique and access to
765 nanomolar variations of NO₃ and DIP in repeated CTD casts, it was possible to demonstrate the role of the ML and exchanges of NO₃ from the ML to the NDLb by vertical advection when variations of MLD occurred simultaneously to transitory accumulation of NO₃ after a deposition event. The time sequence occurring after a wet dust deposition event was summarized Fig. 6 : accumulation of NO₃ in the ML, advection to NDLb, luxury
770 consumption of DIP by hprok and delayed peaks of DIP, decrease of primary production and its recovery after 2 days mainly visible in the nutrient depleted layer. The effect of dust deposition is a complex and time-controlled trophic cascade within the microbial food web. Our study shows the important role of intermittent, but strong abiotic effects such as downwelling advective fluxes from the ML to the nutrient depleted layers. It will be
775 important to consider these aspects on budgets and non-stoichiometric models, especially when climate and anthropogenic changes are predicted to increase aerosol deposition in the Mediterranean Sea.

Data availability

Guieu et al., Biogeochemical dataset collected during the PEACETIME cruise. SEANOE.
780 <https://doi.org/10.17882/75747> (2020).

Author contribution

CG and KD designed the study. FVW measured ectoenzymatic activity and BP, AE managed the TAA analysis and treatments, EP measured DIP with the LWCC technique,
785 CR measured nitrogen fixation, VT assisted in CTD operations and analyzed water

masses, JD sampled for DOC and flow cytometry, FVW prepared the ms with contribution from all co-authors.

Competing interests

790 The authors declare that they have no conflict of interest

Special issue statement

This article is part of the special issue ‘Atmospheric deposition in the low-nutrient–low-chlorophyll (LNLC) ocean: effects on marine life today and in the future (ACP/BG inter-journal SI)’. It is not associated with a conference.

Financial support

The project leading to this publication received funding from CNRS-INSU, IFREMER, CEA, and Météo-France as part of the program MISTRALS coordinated by INSU (doi: 800 10.17600/17000300) and from the European FEDER fund under project no 1166-39417. The research of EM was funded by the Spanish Ministry of Science, Innovation and Universities through grant PGC2018-094553B-I00 (POLARIS).

Acknowledgements. This study is a contribution of the PEACETIME project (805 <http://peacetimoproject.org>, last access 07/04/2021), a joint initiative of the MERMEX and ChArMEx components. PEACETIME was endorsed as a process study by GEOTRACES and is also a contribution to IMBER and SOLAS international programs. The authors thank also many scientists & engineers for their assistance with sampling/analyses: Samuel Albani for NO₃ nanomolar sampling and Maryline Montanes for 810 NO₃ with LWCC technique, Marc Garel, Sophie Guasco and Christian Tamburini for ectoenzymatic activity, Ruth Flerus and Birthe Zancker for TAA, Joris Guittoneau and Sandra Nunige for nutrients, Thierry Blasco for POC, Julia Uitz and Céline Dimier for TChl a (analysed at the SAPIG HPLC analytical service at the IMEV, Villefranche), Philippe Catala for flow cytometry analyses, Barbara Marie and Ingrid Obernosterer for DOC analyses and 815 treatments, Sylvain Triquet and Franck Fu for atmospheric particulate nitrogen and phosphorus. Maurizio Ribera d’Alcalá and a second anonymous reviewer helped much to improve this ms.

References

820 Aminot, A., and Kéroutil, R. : Dosage automatique des nutriments dans les eaux marines, in: Méthodes d'analyses en milieu marin, edited by: IFREMER, Plouzané, 188 pp, ISBN no 978-2-7592-0023-8, 2007.

Bardouki, H., Liakakou, H., Economou, C., Sciare, J., Smolik, J., Zdimal, V., Eleftheriadis, K., Lazaridis, M., Dye, C., and Mihalopoulos, N.: Chemical composition of size resolved atmospheric aerosols in the eastern Mediterranean during summer and winter, *Atmos. Environ.*, 37, 195–208, 2003.

825 Bonnet, S., Grosso, O., and Moutin, T.: Planktonic dinitrogen fixation along a longitudinal gradient across the Mediterranean Sea during the stratified period (BOUM cruise), *Biogeosciences*, 8, 2257–2267, 2011.

830 Bonnet, S., Caffin, M., Berthelot, H., and Moutin, T.: Hot spot of N₂ fixation in the western tropical South Pacific pleads for a spatial decoupling between N₂ fixation and denitrification, *PNAS* letter, doi: 10.1073/pnas.1619514114, 2017.

Brainerd, K. E., and Gregg, M. C.: Surface mixed and mixing layer depths, *Deep-Sea Research Part I*, 42(9), 1521–1543. doi: 10.1016/0967-0637(95)00068-H, 1995.

835 Caffin, M., Berthelot, H., Cornet-Barthaux, V., Barani, A., and Bonnet, S.: Transfer of diazotroph-derived nitrogen to the planktonic food web across gradients of N₂ fixation activity and diversity in the western tropical South Pacific Ocean, *Biogeosciences*, 15, 3795–3810, doi: 10.5194/bg-15-3795-2018, 2018.

Carbo, P., Krom, M. D., Homoky, W. B., Benning, L. G., and Herut, B.: Impact of 840 atmospheric deposition on N and P geochemistry in the southeastern Levantine basin, *Deep Sea Res. II*, 52, 3041–3053. doi: 10.1016/j.dsr2.2005.08.014, 2005.

Céa, B., Lefèvre, D., Chirurgien, L., Raimbault, P., Garcia, N., Charrière, B., Grégoire, G., Ghiglione, J.-F., Barani, A., Lafont, M., and Van Wambeke, F.: An annual survey of bacterial production, respiration and ectoenzyme activity in coastal NW Mediterranean waters: temperature and resource controls, *Environ. Sci. Pollut. Res.*, doi: 10.1007/s11356-014-3500-9, 2014.

845

Christaki, U., Courties, C., Massana, R., Catala, P., Lebaron, P., Gasol, J. M., and Zubkov, M.: Optimized routine flow cytometric enumeration of heterotrophic flagellates using SYBR Green I, *Limnol. Oceanogr. Methods*, 9, doi: 10.4319/lom.2011.9.329, 2011.

850 Cullen, J. J., Franks, P. J., Karl, D. M., and Longhurst, A. L. A. N.: Physical influences on marine ecosystem dynamics. *The sea*, 12, 297-336, 2002.

de Boyer Montegut, C., Madec, G., Fisher, A. S., Lazar, A., and Iudicone, D.: Mixed layer depth over the global ocean: An examination of profile data and a profile-based climatology, *Journal of Geophysical Research. Oceans*, 109, C12003, doi: 855 10.1029/2004JC002378, 2004.

Delmont, T. O., Quince, C., Shaiber, A., Esen, Ö. C., Lee, S. T. M., Rappé, M. R., McLellan, S. L, Lücker, S. and Murat Eren, A.: Nitrogen-fixing populations of Planctomycetes and Proteobacteria are abundant in surface ocean metagenomes, *Nature Microbiology*, doi: 10.1038/s41564-018-0176-9, 2018.

860 Desboeufs, K.: Nutrients atmospheric deposition and variability, in: *Atmospheric Chemistry and its Impacts in the Mediterranean Region* (ChArMex book), Springer, in press.

Desboeufs, K., Bon Nguyen, E., Chevaillier, S., Triquet, S., and Dulac, F.: Fluxes and sources of nutrient and trace metal atmospheric deposition in the northwestern Mediterranean, *Atmospheric Chemistry and Physics*, 18, 14477–14492, doi: 10.5194/acp-18-14477- 865 2018, 2018.

Desboeufs, K., Fu, F., Breassac, M., Tovar-Sánchez, A., Triquet, S., Doussin, J-F., Giorio, C., Siour, G., Rodriguez-Roméro, A., Wagener, T., Dulac, F., and Guieu, C.: Wet deposition of nutrients and trace metals in the remote Western and central Mediterranean Sea: A source for marine biosphere?, *Atmos. Phys. Chem.*, this special issue, in preparation.

870 Dittmar, T.H., Cherrier, J., and Ludwichowski, K.-U: The analysis of amino acids in seawater. In: *Practical Guidelines for the Analysis of Seawater*, edited by: Wurl, O., Boca Raton, FL: CRC-Press, 67–78, 2009.

D'Ortenzio, F., Iudicone, D., de Boyer Montegut, C., Testor, P., Antoine, D., Marullo, S., 875 Santoleri, R., and Madec, G.: Seasonal variability of the mixed layer depth in the

Mediterranean Sea as derived from in situ profiles., *Geophysical Research Letters*, 32, L12605, doi:10.1029/2005GL022463, 2005.

Djaoudi, K., Van Wambeke, F., Barani, A., Hélias-Nunige, S., Sempéré, R., and Pulido-Villena, E.: Atmospheric fluxes of soluble organic C, N, and P to the Mediterranean Sea: potential biogeochemical implications in the surface layer, *Progress in Oceanography*, 163: 59-69, MERMEX special issue, doi: 10.1016/j.pocean.2017.07.008, 2017.

Djaoudi, K., Van Wambeke, F., Coppola, L., D'ortenzio, F., Helias-Nunige, S., Raimbault, P., Taillandier, V., Testor, P., Wagener, T., and Pulido-Villena, E.: Sensitive determination of the dissolved phosphate pool for an improved resolution of its vertical variability in the surface layer: New views in the P-depleted Mediterranean Sea, *Frontiers in Marine Science*, vol 5, article 234, doi: 10.3389/fmars.2018.00234, 2018.

Djaoudi, K., Van Wambeke, F., Barani, A., Bhairy, N., Chevaillier, S., Desboeufs, K., Nunige, S., Labiad, M., Henry des Tureaux, T., Lefèvre, D., Nouara, A., Panagiotopoulos, C., Tedetti, M., and Pulido-Villena E.: Potential bioavailability of organic matter from atmospheric particles to marine heterotrophic bacteria, *Biogeosciences*, 17, 6271–6285, <https://doi.org/10.5194/bg-17-6271-2020>, 2020

Du, C., Liu, Z., Kao, S.-J., and Dai, M.: Diapycnal fluxes of nutrients in an oligotrophic oceanic regime: The South China Sea, *Geophysical Research Letters*, 44, 11, 510–11, 518, doi: 10.1002/2017GL074921, 2017.

Feliú, G., Pagano, M., Hidalgo, P., and Carlotti, F.: Structure and function of epipelagic mesozooplankton and their response to dust deposition events during the spring PEACETIME cruise in the Mediterranean Sea, *Biogeosciences*, 17, 5417–5441, <https://doi.org/10.5194/bg-17-5417-2020>, 2020.

Flaten, G. A., Skjoldal, E. F., Krom, M. D., Law, C. S., Mantoura, F. C., Pitta, P., Psarra, S., Tanaka, T., Tselepidis, A., Woodward, E. M., Zohary, T., and Thingstad, T. F.: Studies of the microbial P-cycle during a Lagrangian phosphate-addition experiment in the Eastern Mediterranean, *Deep-Sea Res II*, 52, 2928–2943, 2005.

Fu, F., Desboeufs, K., Triquet, S., Doussin, J-F., Giorio, C., Dulac, F., and Guieu, C.: Solubility and sources of trace metals and nutrients associated with aerosols collected

900 during cruise PEACETIME in the Mediterranean Sea, *Atmos. Phys. Chem.*, this special issue, in preparation.

910 Galletti, Y., Becagli, S., di Sarra, A., Gonnelli, M., Pulido-Villena, E., Sferlazzo, D. M.,
Traversi, R., Vestri, S., and Santinelli, C.: Atmospheric deposition of organic matter at a
remote site in the Central Mediterranean Sea: implications for marine ecosystem,
Biogeosciences, 17, 3669–3684, <https://doi.org/10.5194/bg-17-3669-2020>, 2020.

Gardner, W. D., Chung, S. P., Richardson, M. J., and Walsh, I. D.: The oceanic mixed-layer
pump, *Deep-Sea Research II* 42, 757-775, 1995.

915 Gasol, J. M., and del Giorgio, P. A.: Using flow cytometry for counting natural planktonic
bacteria and understanding the structure of planktonic bacterial communities, *Scientia
Marina*, 64, 197–224, 2000.

920 Gazeau, F., Van Wambeke, F., Marañon, E., Pérez-Lorenzo, M., Alliouane, S., Stolpe, C.,
Blasco, T., Leblond, N., Zäncker B., Engel A., Marie, B., Dinasquet, J., and Guieu C.:
Impact of dust addition on the metabolism of Mediterranean plankton communities and
carbon export under present and future conditions of pH and temperature,
Biogeosciences Discuss. [preprint], <https://doi.org/10.5194/bg-2021-20>, in review,
2021.

925 Godwin, C. M., and Cotner, J. B.: Aquatic heterotrophic bacteria have highly flexible
phosphorus content and biomass stoichiometry, *the ISME Journal*, 9, 2324–2327,
doi:10.1038/ismej.2015.34, 2015.

Guieu , C., and Ridame, C.: Impact of atmospheric deposition on marine chemistry and
biogeochemistry, in: *Atmospheric Chemistry and its Impacts in the Mediterranean
Region (ChArMex book)*, Springer, in press.

930 Guieu, C., Dulac, F., Desboeufs, K., Wagener, T., Pulido-Villena, E., Grisoni, J.-M., Louis, J.,
Ridame, C., Blain, S., Brunet, C., Bon Nguyen, E., Tran, S., Labiad, M., and Dominici,
J.-M.: Large clean mesocosms and simulated dust deposition: a new methodology to
investigate responses of marine oligotrophic ecosystems to atmospheric inputs,
Biogeosciences, 7, 2765–2784, doi: 10.5194/BG-7-2765-2010, 2010.

935 Guieu, C., Aumont, O., Paytan, A., Bopp, L., Law, C. S., Mahowald, N., Achterberg, E. P.,
Marañón, E., Salihoglu, B., Crise, A., Wagener, T., Herut, B., Desboeufs, K.,
Kanakidou, M., Olgun, N., Peters, F., Pulido-Villena, E., Tovar-Sanchez, A., and
Völker, C.: The significance of episodicity in atmospheric deposition to Low Nutrient
Low Chlorophyll regions, *Global Biogeochem. Cycles*, 28, 1179–1198,
doi:10.1002/2014GB004852, 2014a.

940 Guieu, C., Ridame, C., Pulido-Villena, E., Bressac, M., Desboeufs, K., and Dulac, F.: Impact
of dust deposition on carbon budget: a tentative assessment from a mesocosm approach,
Biogeosciences, 11, 5621–5635, doi: 10.5194/bg-11-5621-2014, 2014b.

945 Guieu, C., D'Ortenzio, F., Dulac, F., Taillandier, V., Doglioli, A., Petrenko, A., Barrillon, S.,
Mallet, M., Nabat, P., and Desboeufs, K.: Process studies at the air-sea interface after
atmospheric deposition in the Mediterranean Sea: objectives and strategy of the
PEACETIME oceanographic campaign (May–June 2017), *Biogeosciences*, 17, 1–23,
2020, doi: 10.5194/bg-17-1-2020.

950 Heimbürger, A., Losno, R., Triquet, S., Dulac F., and Mahowald, N. M.: Direct measurements
of atmospheric iron, cobalt and aluminium-derived dust deposition at Kerguelen
Islands, *Global Biogeochem. Cy.*, 26, GB4016, doi:10.1029/2012GB004301, 2012.

955 Hersbach, H., Bell, B., Berrisford, P., Biavati, G., Horányi, A., Muñoz Sabater, J., Nicolas, J.,
Peubey, C., Radu, R., Rozum, I., Schepers, D., Simmons, A., Soci, C., Dee, D.,
Thépaut, J-N.: ERA5 hourly data on single levels from 1979 to present. Copernicus
Climate Change Service (C3S) Climate Data Store (CDS). doi: 10.24381/cds.adbb2d47,
2018.

Herut, B., Zohary, T., Krom, M. D., Mantoura, R. F. C., Pitta, P., Psarra, S., Rassoulzadegan,
F., Tanaka, T. and Thingstad, T. F.: Response of East Mediterranean surface water to
Saharan dust: On-board microcosm experiment and field observations, *Deep-Sea
Research II* 52 (2005) 3024–3040, 2005.

960 Herut, B., Rahav, E., Tsagaraki, T. M., Giannakourou, A., Tsiola, A., Psarra, S., Lagaria, A.,
Papageorgiou, N., Mihalopoulos, N., Theodosi, C. N., Violaki, K., Stathopoulou, E.,
Scoullos, M., Krom, M. D., Stockdale, A., Shi, Z., Berman-Frank, I., Meador, T. B.,
Tanaka, T., and Paraskevi, P.: The potential impact of Saharan dust and polluted

965 aerosols on microbial populations in the East Mediterranean Sea, an overview of a mesocosm experimental approach, *Front. Mar. Sci.*, 3, 226, doi: 10.3389/fmars.2016.00226, 2016.

Hoppe, H.-G., Ducklow, H., and Karrasch, B.: Evidence for dependency of bacterial growth on enzymatic hydrolysis of particulate organic matter in the mesopelagic ocean, *Mar. Ecol. Prog. Ser.*, 93, 277–283, 1993.

970 Ibello, V., Cantoni, C., Cozzi, S., and Civitarese, G.: First basin-wide experimental results on N₂ fixation in the open Mediterranean Sea, *Geophys. Res. Lett.*, 37, L03608, doi:10.1029/2009GL041635, 2010.

Izquierdo, R., Benítez-Nelson, C. R., Masqué, P., Castillo, S., Alastuey, A., and Ávila, A.: Atmospheric phosphorus deposition in a near-coastal rural site in the NE Iberian Peninsula and its role in marine productivity, *Atmos. Environ.*, 49, 361–370, doi: 10.1016/j.atmosenv.2011.11.007, 2012.

Jumars, P. A., Penry, D. L., Baross, J. A., Perry, M. A., and Frost, B. W.: Closing the microbial loop : dissolved carbon pathway to heterotrophic bacteria from incomplete ingestion, digestion and absorption in animals, *Deep-Sea Research*, 483–495, 1989.

980 Kamykowski, D., and Zentara, S. J.: Nitrate and silicic acid in the world ocean: Patterns and processes, *Mar. Ecol. Prog. Ser.*, 26, 47–59, 1985.

Kanakidou, M., Myriokefalitakis, S., and Tsigaridis, K.: Aerosols in atmospheric chemistry and biogeochemical cycles of nutrients, *Environ. Res. Lett.*, 13, 063004, doi: 10.1088/1748-9326/aabedb, 2018.

985 Kanakidou, M., Myriokefalitakis, S., and Tsagkaraki, M.: Atmospheric inputs of nutrients to the Mediterranean Sea, *Deep Sea Research Part II: Topical Studies in Oceanography*, 171, 104606, doi: 10.1016/j.dsr2.2019.06.014, 2020.

Kirchman, D. L.: Leucine incorporation as a measure of biomass production by heterotrophic bacteria, in: *Handbook of methods in aquatic microbial ecology*, edited by : Kemp, P.F., Sherr, B.F., Sherr, E.B., and Cole, J.J., Lewis, Boca Raton, 509-512, 1993.

Kouvarakis, G., Mihalopoulos, N., Tselepides, T., and Stavrakakis, S.: On the importance of atmospheric nitrogen inputs on the productivity of eastern Mediterranean, *Global Biogeochemical Cycles*, 15, 805–818, doi:10.1029/2001GB001399, 2001.

Krom, M. D., Herut, B., and Mantoura, R. F. C.: Nutrient budget for the eastern
995 Mediterranean: Implication for phosphorus limitation, *Limnol. Oceanogr.*, 49, 1582–1592, doi: 10.4319/lo.2004.49.5.1582, 2004.

Louis, J., Bressac, M., Pedrotti, M.-L., and Guieu, C.: Dissolved inorganic nitrogen and phosphorus dynamics in sea water following an artificial Saharan dust deposition event, *Frontiers Marine Sci.*, 2, article 27, doi: 10.3389/fmars.2015.00027, 2015.

1000 Løvdal, T., Skjoldal, E. F., Heldal, M., Norland, S., and Thingstad, T. F.: Changes in Morphology and Elemental Composition of *Vibrio splendidus* Along a Gradient from Carbon-limited to Phosphate-limited Growth, *Microb. Ecol.*, 55, 152–161, doi: 10.1007/s00248-007-9262-x, 2008.

Makino, W., Cotner, J. B., Sterner, R. W., and Elser, J. J.: Are bacteria more like plants or
1005 animals? Growth rate and resource dependence of bacterial C : N : P stoichiometry, *Functional Ecology*, 17, 121–130, 2003.

Malits, A., Cattaneo, R., Sintes, E., Gasol, J. M., Herndl, G. J., and Weinbauer, M.: Potential impacts of black carbon on the marine microbial community, *Aquat Microb Ecol.*, 75, 27–42, doi: 10.3354/ame01742, 2015.

1010 Marañón, E., Fernández, A., Mouriño-Carballido, B., Martínez-García, S., Teira, E., Cermeño, P., Chouciño, P., Huete-Ortega, M., Fernández, E., Calvo-Díaz, A., Morán, X. A. G., Bode, A., Moreno-Ostos, E., Varela, M. M., Patey, M. D., and Achterberg, E. P.: Degree of oligotrophy controls the response of microbial plankton to Saharan dust, *Limnology and Oceanography*, 55, 2339–2352, 2010.

1015 Marañón, E., Van Wambeke, F., Uitz, J., Boss, E. S., Dimier, C., Dinasquet, J., Angel, A., Haëntjens, N., Pérez-Lorenzo, M., Taillardier, V., and Zäncker, B.: Deep maxima of phytoplankton biomass, primary production and bacterial production in the Mediterranean Sea, *Biogeosciences*, 18, 1749–1767, doi:10.5194/bg-18-1749-2021, 2021.

1020 Mari, X., Guinot, B., Chu, V. T., Brune, J., Lefebvre, J.-P., Pradeep Ram, A. S., Raimbault, P., Dittmar, T., and Niggemann, J.: Biogeochemical Impacts of a Black Carbon Wet Deposition Event in Halong Bay, Vietnam, *Front. Mar. Sci.*, 6, article 185, doi: 10.3389/fmars.2019.00185, 2019.

1025 Marie, D., Simon, N., Guillou, L., Partensky, F., and Vaulot, D.: Flow Cytometry Analysis of Marine Picoplankton, in: *In Living Color: Protocols in Flow Cytometry and Cell Sorting*, edited by: Diamond, R. A., and Demaggio, S., Springer, Berlin, Heidelberg, 421–454, 2000.

1030 Markaki, Z., Loyer-Pilot, M. D., Violaki, K., Benyahya, L., and Mihalopoulos, N.: Variability of atmospheric deposition of dissolved nitrogen and phosphorus in the Mediterranean and possible link to the anomalous seawater N/P ratio, *Marine Chemistry*, 120, 187–194, doi: 10.1016/j.marchem.2008.10.005, 2010.

1035 Martiny, A. C., Pham, C. T. A., Primeau, F. W., Vrugt, J. A., Moore, J. K., Levin, S. A., and Lomas, M. W.: Strong latitudinal patterns in the elemental ratios of marine plankton and organic matter, *Nature geosciences*, 6, 279–283, doi: 10.1038/ngeo1757, 2013.

1040 Mermex Group.: Marine ecosystems' responses to climatic and anthropogenic forcings in the Mediterranean, *Progress in Oceanography*, 91, 97–166, doi: 10.1016/j.pocean.2011.02.003, 2011.

Mescioglu E., Rahav E., Frada M.J., Rosenfeld S., Raveh O., Galletti Y., Santinelli C., Herut B., Paytan A.: Dust-associated airborne microbes affect primary and bacterial production rates, and eukaryote diversity, in the Northern Red Sea: A mesocosm approach. *Atmosphere*, 10, article 358, <https://doi.org/10.3390/atmos10070358>, 2019.

Moreno, A. R., and Martiny, A. C.: Ecological stoichiometry of ocean plankton, *Ann. Rev. Mar. Sci.*, 10, 43–69, 2018.

1045 Moutin, T., and Prieur, L.: Influence of anticyclonic eddies on the Biogeochemistry from the Oligotrophic to the Ultraoligotrophic Mediterranean (BOUM cruise), *Biogeosciences*, 9 (10), 3827 – 3855, doi: 10.5194/bg-9-3827-2012, 2012.

Nagata, T.: Carbon and Nitrogen content of natural planktonic bacteria, *Appl., Environ. Microbiol.*, 52, 28–32, 1986.

1050 Orsini, D., Ma, Y., Sullivan, A., Sierau, B., Baumann, K., and Weber, R.: Refinements to the
Particle-Into-Liquid Sampler (PILS) for Ground and Airborne Measurements of Water
Soluble Aerosol Composition, *Atmospheric Environment*, 37, 1243–1259, 2003.

Omand, M. M. and Mahadevan, A.: The shape of the oceanic nitracline, *Biogeosciences*, 12,
3273–3287, doi: 10.5194/bg-12-3273-2015, 2015.

1055 Pujo-Pay, M., and Raimbault, P.: Improvements of the wet-oxidation procedure for
simultaneous determination of particulate organic nitrogen and phosphorus collected
on filters, *Mar. Ecol. Prog. Ser.*, 105, 203–207, 1994.

Pradeep Ram, A. S., and Sime-Ngando, T.: Resources drive trade-off between viral lifestyles
in the plankton: evidence from freshwater microbial microcosms, *Environ Microbiol*,
12, 467–479, doi: 10.1111/j.1462-2920.2009.02088.x, 2010.

1060 Pulido-Villena, E., Wagener, T., and Guieu, C.: Bacterial response to dust pulses in the
western Mediterranean: Implications for carbon cycling in the oligotrophic ocean,
Global Biogeochem. Cycles, 22, GB1020, doi:10.1029/2007GB003091, 2008.

Pulido-Villena, E., Rérolle, V., and Guieu, C.: Transient fertilizing effect of dust in P-
deficient surface LNLC ocean. *Geophysical Research Letters*, 37, L01603,
1065 doi:10.1029/2009GL041415, 2010.

Pulido-Villena, E., Baudoux, A.-C., Obernosterer, I., Landa, M., Caparros, J., Catala, P.,
Georges, C., Harmand, J., and Guieu, C.: Microbial food web dynamics in response to
a Saharan dust event: results from a mesocosm study in the oligotrophic
Mediterranean Sea, *Biogeosciences*, 11, 337–371, 2014.

1070 Pulido-Villena, E., Desboeufs, K., Djaoudi, K., Van Wambeke, F., Barrillon, S., Doglioli, A.,
Petrenko, A., Taillandier, V., Fu, F., Gaillard, T., Guasco, S., Nunige, S., Triquet, S.,
and Guieu, C.: Phosphorus cycling in the upper waters of the Mediterranean Sea
(Peacetime cruise): relative contribution of external and internal sources,
Biogeosciences Discuss., [preprint], <https://doi.org/10.5194/bg-2021-94>, in review,
1075 2021.

Rahav, E. Herut, B., Levi, A., Mulholland, M. R., and Berman-Frank, I.: Springtime contribution of dinitrogen fixation to primary production across the Mediterranean Sea. *Ocean Sci.* 9, 489–498. doi: 10.5194/os-9-489-2013, 2013a

1080 Rahav, E., Herut, B., Stambler, N., Bar-Zeev, E. Mulholland, M. R., and Berman-Frank, I.: Uncoupling between dinitrogen fixation and primary productivity in the eastern Mediterranean Sea, *J. Geophys. Res. Biogeosci.*, 118, 195–202, doi:10.1002/jgrg.20023, 2013b.

1085 Rahav, E., Paytan, A., Chien, C.-T., Ovadia, G., Katz, T., and Herut, B.: The Impact of Atmospheric Dry Deposition Associated Microbes on the Southeastern Mediterranean Sea Surface Water following an Intense Dust Storm, *Front. Mar. Sci.* 3, 127, doi: 10.3389/fmars.2016.00127, 2016.

1090 Richon, C., Dutay, J. C., Dulac, F., Wang, R., Balkanski, Y., Nabat, P., Aumont, O., Desboeufs, K., Laurent, B., Guieu, C., Raimbault, P., and Beuvier, J.: Modeling the impacts of atmospheric deposition of nitrogen and desert dust-derived phosphorus on nutrients and biological budgets of the Mediterranean Sea, *Prog. Oceanogr.* 163, 21–39, doi: 10.1016/j.pocean.2017.04.009, 2018.

Ridame, C., Moutin, T., and C. Guieu.: Does phosphate adsorption onto Saharan dust explain the unusual N/P ratio in the Mediterranean Sea? *Oceanologica Acta*, 26, 629–634, doi: 10.1016/S0399-1784(03)00061-6, 2003.

1095 Ridame, C., Le Moal, M., Guieu, C. Ternon, E., Biegala, I., L'Helguen, S., and Pujo-Pay, M.: Nutrient control of N₂ fixation in the oligotrophic Mediterranean Sea and the impact of Saharan dust events, *Biogeosciences*, 8, 2773–2783, doi:10.5194/bg-8-2773-2011, 2011.

1100 Sala, M. M., Peters, F., Gasol, J. M., Pedros-Alio, C., Marrasse, C., and Vaque, D.: Seasonal and spatial variations in the nutrient limitation of bacterioplankton growth in the northwestern Mediterranean, *Aquat. Microb. Ecol.*, 27, 47–56, 2002.

Sandroni, V., Raimbault, P., Migon, C., Garcia, N., and Gouze, E.: Dry atmospheric deposition and diazotrophy as sources of new nitrogen to northwestern Mediterranean oligotrophic surface waters, *Deep-Sea Res. I*, 54, 1859–1870, doi:10.1016/j.dsr.2007.08.004, 2007.

1105 Taillardier, V., Prieur, L., D'Ortenzio, F., Ribera d'Alcalà, M., and Pulido-Villena, E.: Profiling float observation of thermohaline staircases in the western Mediterranean Sea and impact on nutrient fluxes, *Biogeosciences*, 17, 3343–3366, 2020.

1110 Talarmin A, Van Wambeke F., Lebaron P., and Moutin T.: Vertical partitioning of phosphate uptake among picoplankton groups in the low Pi Mediterranean Sea, *Biogeosciences*, 12: 1237–1247 doi:10.5194/bg-12-1237-2015, 2015.

Tanaka, T., Thingstad, T. F., Christaki, U., Colombe, J., Cornet-Barthaux, V., Courties, C., Grattepanche, J.-D., Lagaria, A., Nedoma, J., Oriol, L., Psarra, S., Pujo-Pay, M., and Van Wambeke, F.: Lack of P-limitation of phytoplankton and heterotrophic prokaryotes in surface waters of three anticyclonic eddies in the stratified Mediterranean Sea, *Biogeosciences*, 8, 525–538, doi: 10.5194/bg-8-525-2011, 2011.

1115 Tovar-Sánchez, A., Rodríguez-Romero, A., Engel, A., Zäncker, B., Fu, F., Marañón, E., Pérez-Lorenzo, M., Bressac, M., Wagener, T., Triquet, S., Siour, G., Desboeufs, K., and Guieu, C.: Characterizing the surface microlayer in the Mediterranean Sea: trace metal concentrations and microbial plankton abundance, *Biogeosciences*, 17, 2349–2364, <https://doi.org/10.5194/bg-17-2349-2020>, 2020.

1120 Thingstad, T., Krom, M. D., Mantoura, F., Flaten, G., Groom, S., Herut, B., Kress, N., Law, C. S., Pasternak, A., Pitta, P., Psarra, S., Rassoulzadegan, F., Tanaka, T., Tselepides, A., Wassmann, P., Woodward, M., Riser, C., Zodiatis, G., and Zohary, T.: Nature of phosphorus limitation in the ultraoligotrophic eastern Mediterranean, *Science*, 309, 1068–1071, doi: 10.1126/science.1112632, 2005.

1125 Van Wambeke, F., Christaki, U., Giannakourou, A., Moutin, T., and Souvmerzoglou, K.: Longitudinal and vertical trends of bacterial limitation by phosphorus and carbon in the Mediterranean Sea, *Microb. Ecol.*, 43, 119–133, doi: 10.1007/s00248-001-0038-4, 2002.

1130 Van Wambeke, F., Gimenez, A., Duhamel, S., Dupouy, C., Lefevre, D., Pujo-Pay, M., and Moutin, T.: Dynamics and controls of heterotrophic prokaryotic production in the western tropical South Pacific Ocean: links with diazotrophic and photosynthetic activity, *Biogeosciences*, 15: 2669–2689, doi: 10.5194/bg-15-2669-2018, 2018.

Van Wambeke, F., Pulido-Villena, E., Catala, P., Dinasquet, J., Djaoudi, K., Engel, A., Garel, 1135 M., Guasco, S., Marie, B., Nunige, S., Taillandier, V., Zäncker, B., and Tamburini, C.:
Spatial patterns of ectoenzymatic kinetics in relation to biogeochemical properties in
the Mediterranean Sea and the concentration of the fluorogenic substrate used,
Biogeosciences, 18, 2301-2323, doi:10.5194/bg-18-2301-2021, 2021.

Yelton, A. P., Acinas, S. G., Sunagawa, S., Bork, P., Pedros-Alio, C., Chisholm, S. W.:
1140 Global genetic capacity for mixotrophy in marine picocyanobacteria, ISME J 10:2946-
2957, 2016.

Zhang, J.-Z., and Chi, J.: Automated analysis of nano-molar concentrations of phosphate in
natural waters with liquid waveguide, Environ. Sci. Technol., 36, 1048–1053, doi :
10.1021/es011094v, 2002.

1145

Table 1. Main biogeochemical features/trophic conditions during the PEACETIME cruise. For TYR, ION and FAST sites investigated over several days, means \pm sd are indicated. ITChla: Integrated total chlorophyll a (Chla + dvChla). IPP: Integrated particulate primary production; IBP: integrated heterotrophic prokaryotic production. Integrations from surface to 200 m depth for all data expect IPP, integrated down to the depth of 1% Photosynthetically Active Radiation (PAR) level.

	sampling date	Lat. °N	Long. °E	Temp. at 5 m °C	Bottom depth m	DCM depth m	ITChl a mg chla m ⁻²	IPP mg C m ⁻² d ⁻¹	IBP mg C m ⁻² d ⁻¹
ST1	May 12	41°53.5	6°20	15.7	1580	49	35,0	284	51
ST2	May 13	40°30.36	6°43.78	17.0	2830	65	32,7	148	55
ST3	May 14	39°0.8.0	7°41.0	14.3	1404	83	23,2	140	77
ST4	May 15	37°59.0	7°58.6	19.0	2770	64	29,2	182	66
ST5	May 16	38°57.2	11°1.4	19.5	2366	77	30,5	148	51
TYR	May 17-20	39°20.4	12°35.56	19.6	3395	80 \pm 6	29 \pm 3	170 \pm 35	57 \pm 3
ST6	May 22	38°48.47	14°29.97	20.0	2275	80	18,7	142	62
ST7	May 24	36°39.5	18°09.3	20.6	3627	87	24.2	158	57
ION	May 25-28	35°29.1	19°47.77	20.6	3054	97 \pm 5	29 \pm 2	208 \pm 15	51 \pm 9
ST8	May 30	36°12.6	16°37.5	20.8	3314	94	31.6	206	71
ST9	June 2	38°08.1	5°50.5	21.2	2837	91	36.1	214	64
FAST	June 2-7 and 9	37°56.8	2°54.6	21.0	2775	79 \pm 8	34 \pm 8	211 \pm 57	92 \pm 11
ST10	June 8	37°27.58	1°34.0	21.6	2770	89	28,9	nd	96

1155 **Table 2.** N budget at the short stations within the surface mixed layer (ML). Integrated stocks
 (NO₃, $\mu\text{mol N m}^{-2}$) and fluxes (heterotrophic prokaryotic N demand (hprokN demand),
 phytoplankton N demand (phytoN demand), in situ leucine aminopeptidase hydrolysis fluxes
 (LAP), dry atmospheric deposition of NO₃ and NH₄ (all fluxes in $\mu\text{mol N m}^{-2} \text{ d}^{-1}$). Values
 presented as mean \pm sd. SD was calculated using propagation of errors: For hprokN demand
 triplicate measurements at each depth and a C/N ratio of 7.3 ± 1.6 ; for phytoN demand
 1160 triplicate measurements of PP at each depth and a C/N ratio of 7 ± 1.4 ; for LAP the analytical
 TAA error and the V_m and K_m errors; for N₂fix the coefficient of variation was 10% for
 volumetric fluxes $> 0.1 \text{ nmole N l}^{-1} \text{ d}^{-1}$ and 20% for lower values. For dry deposition, sd is
 based on the variability of the NO₃ and NH₄ concentrations solubilized from aerosols during
 the occupation of the station (see methods section 2.2.1). MLD: mixed layer depth. na: not
 1165 available because under LWCC detection limits.

stations	MLD	stocks	biological fluxes				Dry deposition	
			phytoN demand	hprokN demand	LAP	N ₂ fixation	NO ₃	NH ₄
m		$\mu\text{mol N m}^{-2}$	$\mu\text{mol N m}^{-2} \text{ d}^{-1}$					
ST1	21	na	1468 \pm 325	184 \pm 40	121 \pm 28	14.6 \pm 1.5	18.6 \pm 1.4	1.5 \pm 0.3
ST2	21	na	481 \pm 161	163 \pm 35	48 \pm 24	10.7 \pm 1.1	23.7 \pm 2.2	4.1 \pm 0.9
ST3	11	na	282 \pm 82	126 \pm 28	40 \pm 17	7.8 \pm 0.8	33.8 \pm 3.6	4.7 \pm 0.5
ST4	15	na	246 \pm 80	132 \pm 28	83 \pm 20	10.7 \pm 1.1	23.8 \pm 2.9	6.3 \pm 2.6
ST5	9	261 \pm 22	112 \pm 29	42 \pm 9	17 \pm 12	4.8 \pm 0.5	27.0 \pm 7.5	7.9 \pm 1.8
ST6	18	162 \pm 14	410 \pm 116	204 \pm 44	48 \pm 24	9.1 \pm 0.9	15.0 \pm 0.6	9.3 \pm 0.7
ST7	18	162 \pm 14	226 \pm 123	148 \pm 33	83 \pm 18	10.5 \pm 1.1	23.6 \pm 1.9	8.0 \pm 1.2
ST8	14	911 \pm 77	274 \pm 66	130 \pm 33	25 \pm 8	4.3 \pm 0.5	13.4 \pm 1.7	3.8 \pm 0.6
ST9	7	819 \pm 70	259 \pm 70	85 \pm 22	21 \pm 6	3.4 \pm 0.4	27.4 \pm 3.8	13.5 \pm 0.8
ST10	19	2074 \pm 176	495 \pm 31	294 \pm 64	42 \pm 26	13.6 \pm 1.4	23.9 \pm 3.4	4.1 \pm 0.4

1170 **Table 3.** Characteristics and nutrient fluxes estimated in the 2 rains collected during the PEACETIME cruise at ION and FAST sites.

event	Rain ION	Rain FAST
Date and local time	29/05 05:08-6:00	05/06 02:36-3:04
Estimated precipitation (mm)	3.5 ± 1.2	5.7 ± 1.4
DIP Flux nmol P m ⁻²	663 ± 227	1146 ± 290
DOP Flux nmol P m ⁻²	974 ± 334	908 ± 230
POP fluxes nmol P m ⁻²	239 ± 82	8801 ± 2227
NO ₃ Flux $\mu\text{mol N m}^{-2}$	67 ± 22	341 ± 86
NH ₄ Flux $\mu\text{mol N m}^{-2}$	71 ± 24	208 ± 53
DIN Flux $\mu\text{mol N m}^{-2}$	138 ± 47	550 ± 139

Figure legends

1175 **Figure 1.** Nitrate (NO_3) aerosol concentration along the PEACETIME transect. The locations of two rain events are indicated by large black circles. Stations ST 1 to 4 were not sampled for nutrient analysis at a nanomolar level.

Figure 2. Representation of the mixed layer (ML), the bottom of the nitrate (NO_3) depleted layer (NDLb), delineated by the nitracline depth and the mixed layer depth (MLD).

1180 **Figure 3.** a) Evolution of the wind speed during the PEACETIME cruise. The stations are indicated in yellow and dates in black. Vertical dotted lines delineate the beginning and the end of the ship's deployment at TYR, ION and FAST sites. The two rain events collected on board are indicated in solid vertical red arrows and surrounding observed rain events by horizontal dashed red arrows. b) 0-100 m vertical distribution of nitrate (NO_3) with depth.

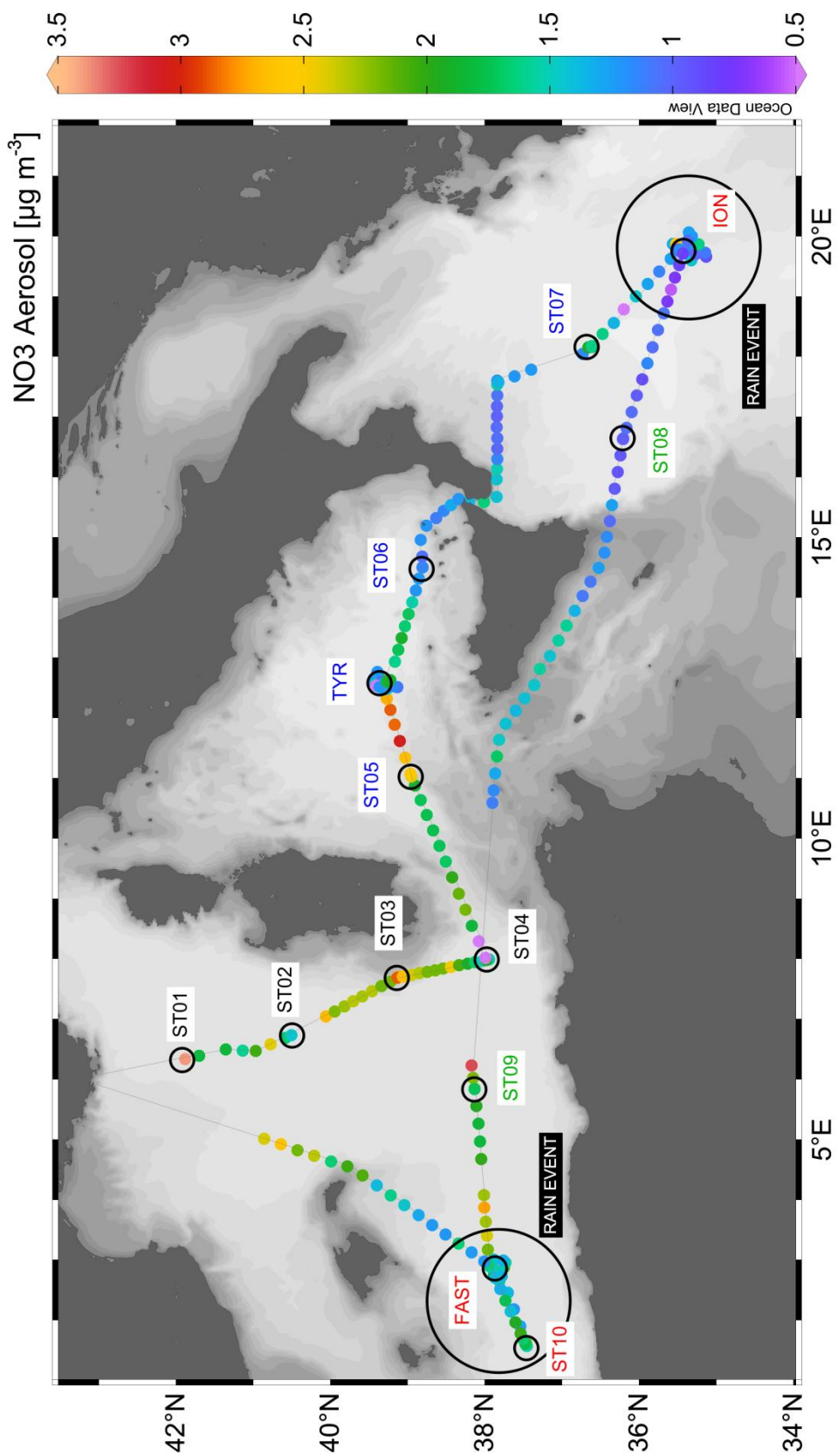
1185 The MLD (in red) and nitracline (in brown) are indicated.

Figure 4. Average concentration of nitrate (NO_3) in the ML and the NDLb, and NO_3 flux from the ML to NDLb. The stations have been classified into 4 types (1 in blue, 2 in green, 3 in yellow, 4 in red, see section Results and Table S1 for definitions). Error bars are indicated by standard deviation around average values for nitrate concentrations, and error propagation 1190 for the flux from ML to NDLb using a 0.5 m uncertainty in the MLD variation.

Figure 5. Evolution within the ML of heterotrophic prokaryotic production (BP), particulate primary production (PP), heterotrophic prokaryotes (hprok) and *Synechococcus* (syn) abundances at the FAST site. The mixed layer depth is indicated by a red line.

1195 **Figure 6.** Synthetic view of biogeochemical processes and exchanges between the ML and NDLb at the FAST site before the rain and evolution after the rain.

Fig. 1



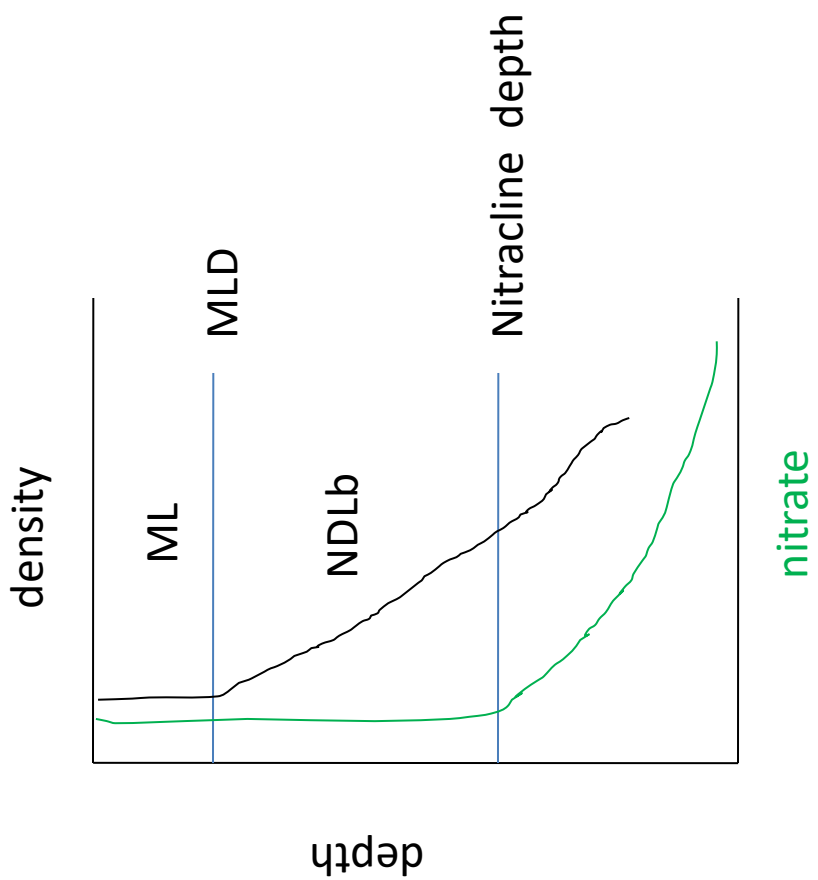


Fig.2

Fig. 3

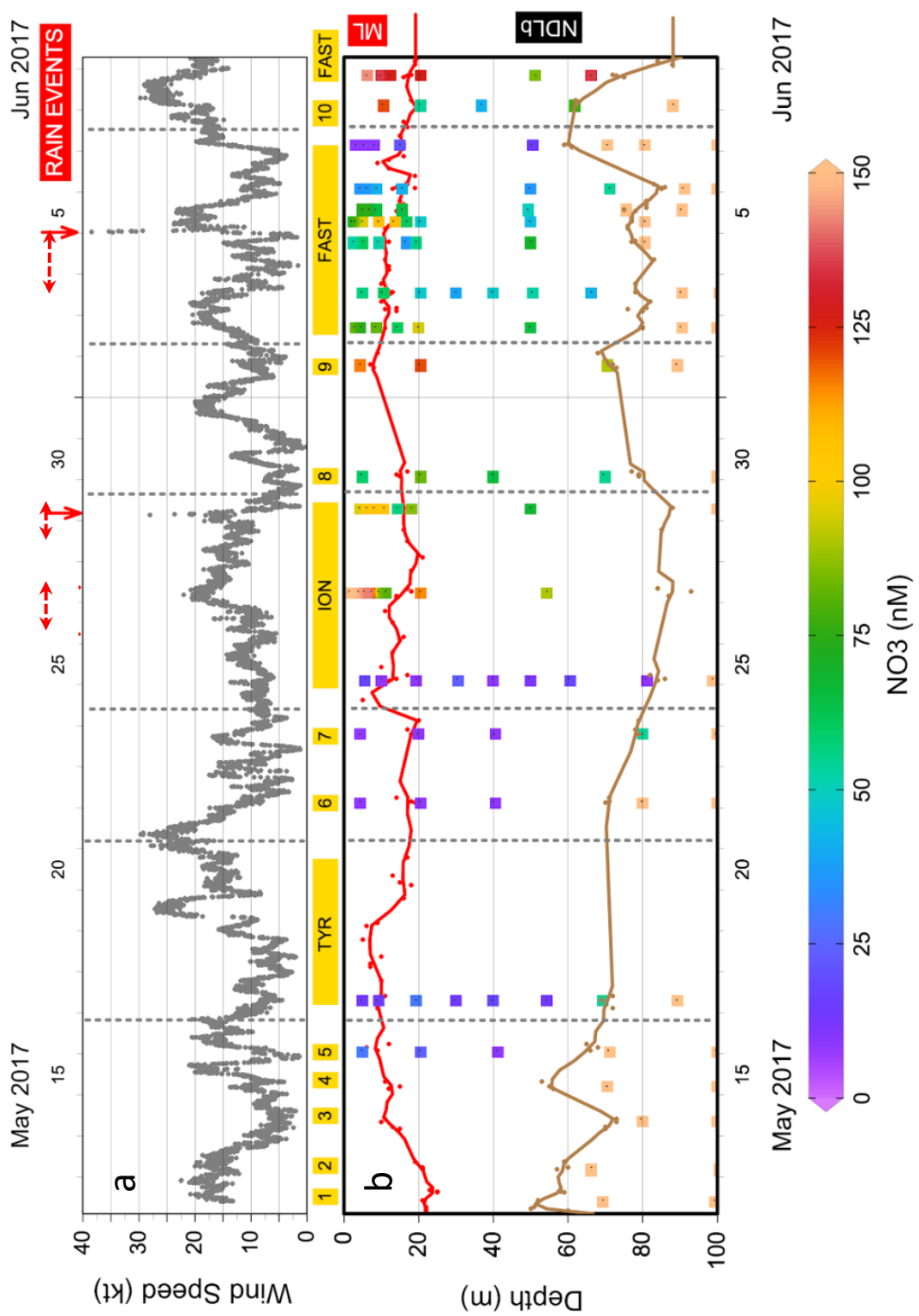


Fig. 4

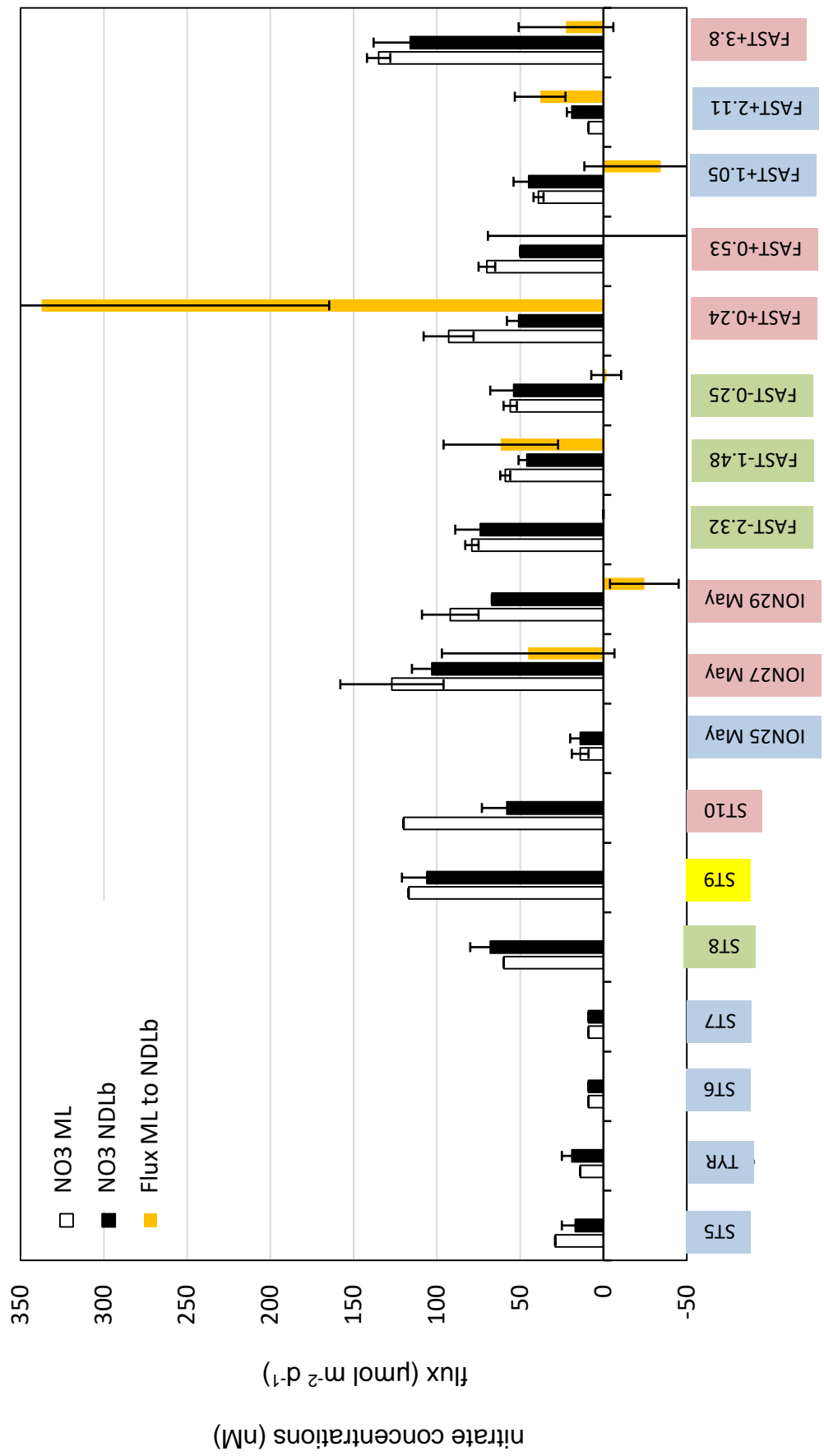


Fig. 5

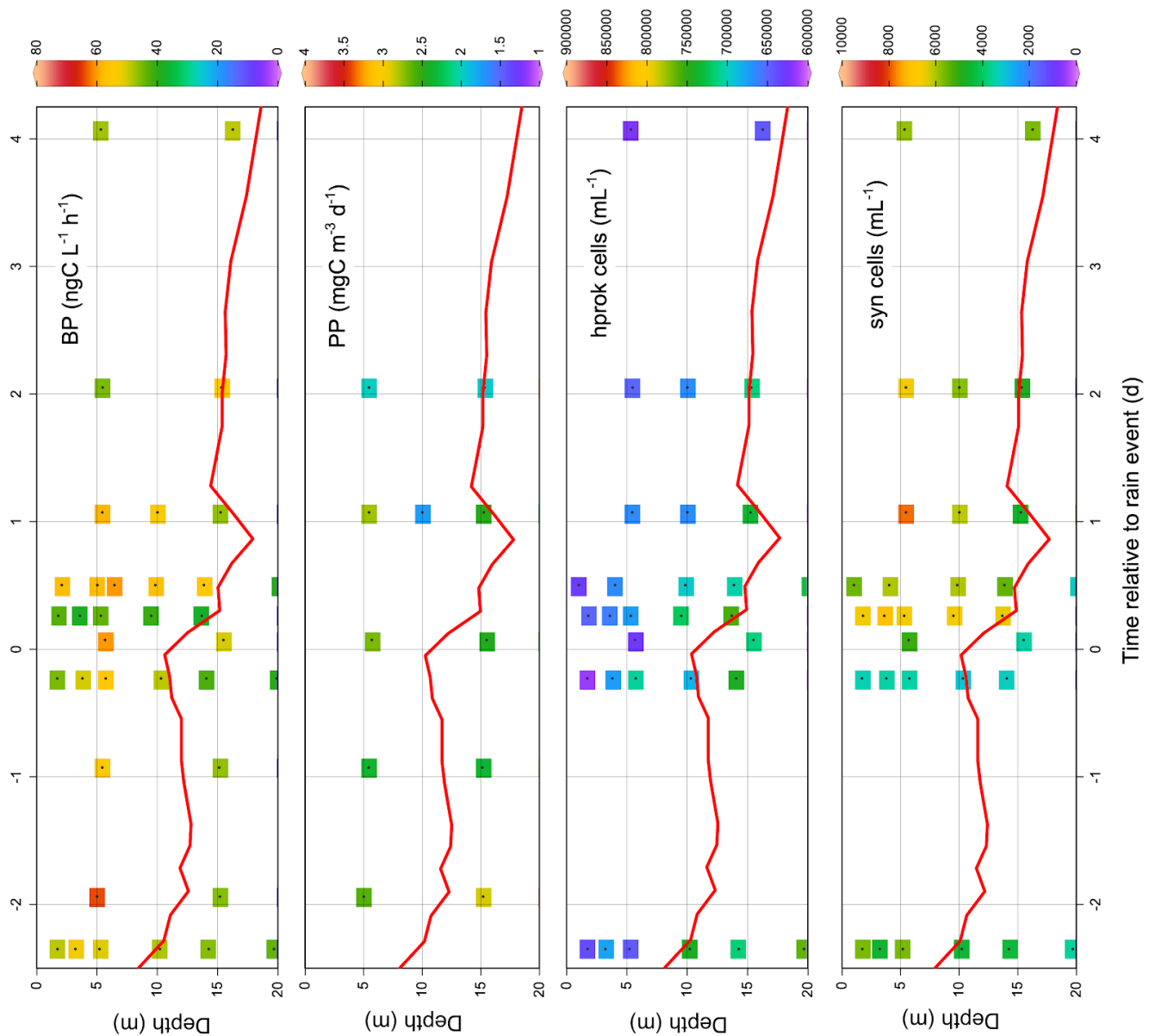


Fig. 6

